Drug Design, Development and Therapy

Dovepress

open access to scientific and medical research

Open Access Full Text Article

REVIEW

Revisiting Niclosamide Formulation Approaches – a Pathway Toward Drug Repositioning

Mario Jug[1], Flavia Laffleur[2], Gioconda Millotti[3]

[1]Department of Pharmaceutical Technology, Faculty of Pharmacy and Biochemistry, University of Zagreb, Zagreb, 10 000, Croatia; [2]Department of Pharmaceutical Technology, Institute of Pharmacy, Center for Molecular Biosciences Innsbruck, University of Innsbruck, Innsbruck, 6020, Austria; [3]Faculty of Natural Sciences, Juraj Dobrila University of Pula, Pula, 52100, Croatia

Correspondence: Gioconda Millotti, Faculty of Natural Sciences, Juraj Dobrila University of Pula, Zagrebačka 30, Pula, 52100, Croatia, Email gmillotti@unipu.hr

Abstract: Niclosamide (NIC), an anthelmintic drug, has garnered recent attention for its potential as an antiviral, antibacterial, and chemotherapeutic agent, among other applications. Repurposing NIC presents a current trend, offering significant time and cost savings compared to developing entirely new therapeutic chemical entities. However, its drawback lies in poor solubility, resulting in notably low oral bioavailability. This review consolidates efforts to overcome this limitation by summarizing twelve categories of formulations, spanning derivatives, amorphous solid dispersions, co-crystals, nanocrystals, micelles, nanohybrids, lipid nanoparticles and emulsions, cyclodextrins, polymeric nanoparticles, dry powders for inhalation, 3D printlets, and nanofibers. These formulations cover oral, injectable, inhalable and potentially (trans)dermal routes of administration. Additionally, we present a comprehensive overview of NIC characteristics, including physico-chemical properties, metabolism, safety, and pharmacokinetics. Moreover, we identify gaps in formulation and administration pathways that warrant further investigation to address NIC poor bioavailability.

Keywords: niclosamide, drug repurposing, solubility, formulations, administration pathways, pharmaco-kinetics

Introduction

Niclosamide (NIC) is a generic anthelmintic drug approved by the Food and Drug Administration (FDA) which is listed in the Model List of Essential Medicines produced by the World Health Organization (WHO).[1] In recent years, there has been a consistent increase in the popularity of studies exploring the potential of niclosamide for various diseases, such as cancer, bacterial infections, and viral infections.[2] It was suggested that its anti-tumor activity involves blocking multiple pathways (WNT/b-catenin, mTORC1, Stat3, NF-kB, Notch) and inducing cell-cycle arrest through targeting mitochondrial enzymes, resulting in growth inhibition and programmed cell death.[3] In 2004, Wu et al reported inhibitory effect of NIC on viral replication of SARS-CoV. A more recent study in 2019 demonstrated that niclosamide is highly effective in inhibiting the viral replication of MERS-CoV by over a 1000-fold, positioning it as a promising agent against viral replication.[4,5] In recent years, a great effort to repurpose niclosamide has been made. Drug repurposing involves identifying new therapeutic applications for drugs that have already received approval, in order to minimize pharmaceutical research expenses[6.] Nevertheless, the primary constraint linked to NIC is its low water solubility, leading to restricted bioavailability.[7] Improving water solubility is key for repurposing of NIC. Numerous strategies can be employed to improve the aqueous solubility and dissolution rate of an Active Pharmaceutical Ingredient (API). These approaches include particle size reduction, co-crystals, salts, amorphous solid dispersion, cyclodextrins, co-solvents, surfactants, lipid-based formulations, and others.[8] This review outlines the endeavors made to enhance the water solubility and consequently the bioavailability of NIC, considering various formulation strategies and administration pathways.

Received: 11 April 2024
Accepted: 5 August 2024
Published: 17 September 2024

NIC Properties

Physicochemical Properties of NIC

NIC (5-chloro-N-(2-chloro-4-nitrophenyl)-2-hydroxybenzamide) is a crystalline solid with a yellowish-grey hue and odourless nature, melting within the temperature range of 224 to 229 °C.[8] The solubility of NIC at 20 °C has been reported to be 5–8 μg/mL.[2] For its properties of low solubility and high permeability, NIC has been classified as a class II drug in the Biopharmaceutical Classification System (BCS), meaning that its bioavailability is limited by the dissolution rate.[2] NIC, classified as a weak acid, contains an ionizable phenolic -OH group, with reported *pKa* values ranging from 5.6 to 7.2. Consequently, the solubility of NIC and *Log D* is heightened at higher pH conditions.[2,9] At a blood pH of 7.4, NIC predominantly exists in its anionic form. There are two obstacles hindering the oral absorption of NIC. Firstly, as a weak acid, NIC remains neutral at low pH levels, limiting its solubility in the gastric region. Secondly, while the higher pH in the small intestine enhances its solubilization, the permeation through enterocyte membranes becomes less favourable due to the increased proportion of charged species.[10] Moreover, it has been reported that there is no significant difference in solubility between the acidic medium (0.1N HCl) and buffered medium (pH 6.8). This finding further exacerbates the challenge of absorption.[11] Another significant aspect concerning pH is that when NIC in amorphous solid dispersion is exposed to acidic media, it undergoes crystallization.[9] This results in even poorer dissolution and subsequently lowers the bioavailability of NIC. Additionally, NIC experiences chemical degradation in both acidic and basic conditions, attributed to hydrolysis.[9] Furthermore, some reports have indicated that alkaline solutions promote the photooxidation of NIC.[12] The degradation products of NIC exhibit toxicity to mononuclear cells, neuronal cells, and alveolar cell lines, while demonstrating non-toxicity to hepatic cell lines.[13] *Log P* was reported to be 3.91[2]. NIC, due to its *pKa* and *LogP* values, demonstrates an affinity for and accumulates within acidic environments, including cancer cells and acidic intracellular vesicles.[2] Research indicates an efficient distribution of NIC from the bloodstream to tumours, where it attains concentrations in the micromolar range.[14]

Besides being poorly water-soluble, it also exhibits poor glass-forming characteristics.[1] The evaluation of a drug's tendency to become amorphous is determined by its glass-forming ability (GFA), which is classified into three categories: poor (class 1), modest (class 2), and good (class 3). NIC falls under class 1, indicating a high propensity for recrystallization, implying it cannot naturally form an amorphous solid. However, it has the potential to create an amorphous solid dispersion or glass solution when dissolved in a solid matrix.[1] Glassy materials possess higher thermodynamic energy compared to crystalline ones, resulting in enhanced solubility and dissolution rates.[9] As mentioned earlier, a low pH environment promotes the conversion of the amorphous form to the crystalline form.

The literature describes three crystal forms of NIC: a hygroscopic anhydrous form, along with two monohydrates named H_A and H_B.[15] In an aqueous medium, the anhydrous form swiftly transforms into H_A, and subsequently transitions to the most stable and least water-soluble form, H_B.[10] Indeed, the solubility decreases from 13.32 μg/mL in the anhydrous form to 0.95 μg/mL and 0.61 μg/mL for the monohydrates H_A and H_B.[10] Jara et al reported that the transition of NIC anhydrate to NIC H_A during storage can be visually confirmed, as the original yellowish-white powder of NIC anhydrate turns yellow in the H_A form.[2] Therefore, it was recommended to subject NIC to treatment at 100 °C for 15 minutes if the raw material is exposed to high humidity.[15] While both NIC anhydrate and monohydrate are options for drug formulation, each presents drawbacks. The anhydrate exhibits a high affinity for water, whereas the hydrate's poorer solubility can lead to sedimentation during storage.[15] NIC possesses several potential hydrogen-bonding sites, including NO_2, OH, and carbonyl groups, along with two Cl atoms capable of forming halogen bonds. These structural characteristics generally promote the formation of solvates and co-crystals, offering promising avenues for enhancing solubility and decreasing hygroscopicity.[16] The *LogP* value for NIC reveals its solubility being thousands of times higher in the organic phase than in the aqueous phase, indicating a preference for lipid dissolution, membrane penetration, and protein binding. However, at pH 6.9, the *LogD* (referring to lipophilicity at a specific pH) value of 3.6 suggests a declining trend in lipid partitioning due to increased ionization. Nevertheless, its significant lipophilicity could still encourage the development of lipid-based formulations.[17,18] The most effective formulations are likely to generate moderate supersaturation close to the site of absorption. Lipid-based formulations are particularly well suited to these criteria since solubilization protects

against high supersaturation ratios (and precipitation), and supersaturation initiation typically occurs in the small intestine at the absorptive membrane.[19]

NIC Plasma Protein Binding, Permeability, Metabolism, CYP Inhibition and Safety

A recent study revealed that NIC, at concentrations of 1 and 10 μM, displayed an extensive binding affinity to plasma proteins, surpassing 99% in both rat and human plasma. This significant plasma protein binding raises considerable concerns regarding potential drug-drug interactions. With multiple drugs co-administered, there's a risk of competition for the same binding sites, potentially altering free drug concentrations and subsequent therapeutic outcomes.[20] The permeability of NIC (1μM) was assessed using Caco-2 cells in the apical to basolateral direction (AB→BL), revealing a P_{app} value of 28.33×10^{-6} cm/s. Notably, NIC permeability closely resembles that of the control with high permeability, propranolol (27.5×10^{-6} cm/s), rather than the control for low permeability, atenolol (1.75×10^{-6}).[20] The same research group further investigated the efflux ratio ($P_{app\ BL\rightarrow AP}$ / $P_{app\ AP\rightarrow BL}$). The ratio was determined to be 0.98, indicating no involvement of efflux transporters. Consequently, intestinal permeability is unlikely to be a contributing factor to the low bioavailability.[20] Nevertheless, as the concentration of NIC increased to 10 μM, the P_{app} value dropped by 10-fold (2.90×10^{-6} cm/s), indicating that its low solubility might impede intestinal absorption.[20]

NIC undergoes significant Phase I metabolism by Cytochrome P450 enzymes (CYP), with notable Phase II metabolism by UDP-glycuronosyltransferases (UGTs). The primary metabolizers for both phases I and II are CYP1A2, primarily located in the liver, and UGT1A1, predominantly found in the liver and small intestine. CYP1A2 catalyzes the formation of 3-hydroxy NIC metabolites, while UGT1A1 generates the NIC-2-O-glucuronide metabolite.[2,21] The production of 3-hydroxy NIC in the liver is minimal compared to the synthesis of NIC-2-O-glucuronide in both the intestine and liver.[22] Therefore, the primary metabolic pathway for NIC is intestinal and hepatic glucuronidation, with the intestinal metabolism rate being approximately 10 times higher than hepatic metabolism. This indicates that UGT metabolization might significantly contribute to the reduced bioavailability of NIC.[2] The distribution and relative abundance of these enzymes vary across different tissues and animal models.[21,22] Among dogs, monkeys, mice, and rats, microsomes in monkeys exhibit glucuronidation parameters that are closest to humans.[21]

The half-lives of NIC in rat, dog, and human hepatic microsomes were determined to be 44.9, 16.0, and 11.8 minutes, respectively. These results suggest that NIC is metabolically unstable, with a half-life of approximately 45 minutes, and that the half-life tends to be shorter in larger mammals.[23] This also indicates that human metabolization is more challenging and complex with respect to preclinical models.[2] In humans, these enzymes are predominantly localized in the liver, colon, and small intestine.[24] While in rats and mice, being the most common animal models, NIC primarily targets the liver and small intestine during its biodistribution.[25,26] Several studies have observed a second peak in the plasma concentration profile following both oral and intravenous administration of NIC. Some authors have linked this phenomenon to enterohepatic circulation. Molecules exhibiting this phenomenon typically display multiple peaks in their pharmacokinetic profiles. However, only a few formulations of NIC have demonstrated this behavior. It remains unclear whether NIC undergoes enterohepatic circulation.[10]

In a study conducted by Seo et al[20] the impact of NIC on seven CYP isoenzymes was examined. Results indicated that NIC showed negligible inhibitory activity on most of the tested isoenzymes, except for CYP1A2 and CYP2C8. The IC_{50} values for these two isoenzymes were found to be 6.66 uM and 6.34 uM, respectively, signifying that NIC has a potent inhibitory effect on these specific CYP enzymes. Therefore, it is essential to highlight the need for careful consideration of potential drug-drug interactions mediated by CYP enzymes, particularly those involving these two isoforms.[20] The authors concluded that NIC is improbable to display time-dependent inhibitory effects on CYP1A2 and CYP2C8. Consequently, careful consideration is crucial when selecting drugs for co-medication with NIC to prevent adverse reactions.

Regarding NIC safety, several studies have reported that the oral administration of NIC is safe.[2] However, clinical trials also present conflicting findings. For instance, in their review, Jara and Williams[2] reported differing maximum tolerated doses. In the phase I clinical trial NCT02532114 of 2018, Schweizer et al observed that patients tolerated doses of up to 500 mg three times daily (TID), totaling 1500 mg/day in solid capsule form. Furthermore, it was concluded by the authors that the administered dose of NIC *per os* (PO) should not be above 500 mg TID.[27] Conversely, in the

subsequent phase Ib clinical trial conducted by Parikh et al in 2021 (NCT02807805), patients were administered 1200 mg of a NIC formulation orally twice a day, reporting favorable patient tolerance.[28] However, it must be noted that in the above-cited studies, NIC was administered along with another drug (enzalutamide and abiraterone/prednisone, respectively).

It can be said that safety profile of systemic delivery of NIC remains largely unexplored, necessitating future studies for a clearer understanding of its toxicity. The oral dose of NIC as a cestocidal agent is 2g as a single dose, resulting in a wide range of serum concentrations due to variable absorption rates. Consequently, the efficacy of clinical studies is unpredictable due to low oral bioavailability and substantial variations in serum concentrations. Further investigations utilizing formulations with high bioavailability are necessary before NIC can be more widely utilized.[29]

Pharmacokinetics of NIC

Pharmacokinetic data was collected from a study conducted by Choi et al, where NIC was administered to rats and dogs via intravenous (IV), oral (PO), and intramuscular (IM) routes at various doses.[23] The dosing solutions were prepared using a solvent mixture comprising 10% DMSO, 30% PEG, 20% of 0.05N NaOH, and 40% saline.[23] Following intravenous (IV) administration to rats, the authors observed that increasing the nominal dose of NIC by 3.3 and 10 times led to dose-dependent increases in C_{max} and AUC_{last}, specifically by 3.0 and 11.5 times, respectively. The clearance (CL) values were moderate compared to the hepatic blood flow rate of rats and did not show significant changes with the NIC dose. This implies that NIC was primarily confined to the plasma pool with limited tissue distribution due to its high plasma-protein binding properties. Indeed, the authors found that plasma protein binding in rat, dog, and human plasma samples was remarkably high, with values of 99.86% ± 0.006%, 99.83% ± 0.015%, and 99.84% ± 0.042%, respectively.[23] This is in accordance with Seo et al[20] NIC presented a linear pharmacokinetic profile in an IV gavage. In rats, the oral bioavailability of NIC was measured at 5.51% ± 1.02%, with very low plasma exposure, suggesting limited absorption. This is the result of the moderate clearance (CL) value in comparison to the hepatic blood flow rate of rats. The authors stated that NIC presented flip-flop kinetics. This implies that the rate of absorption is lower compared to the rate of elimination. Conversely, the absorption rate of NIC via intramuscular (IM) administration in rats was high, with a T_{max} of 5 minutes, and the bioavailability was higher than that achieved via oral (PO) administration.

In dogs, following intravenous (IV) administration, a high mean clearance (CL) was observed, along with a low volume of distribution at steady state (V_{ss}), indicating poor distribution of NIC in tissues. Additionally, after oral administration, flip-flop kinetics were observed, and the oral bioavailability of NIC was only 0.54%, attributed to the high CL value.

Regarding biodistribution, NIC initially accumulates in the intestines, kidneys, liver, and spleen. Levels of NIC in the heart and lungs are negligible following intravenous (IV) administration after an IV administration in rats (2 mg/kg).[2,25] On the other hand, after oral administration of NIC ethanolamine to mice, Tao et al observed that the biodistribution of the NIC salt was higher in the liver and kidneys, with lower levels detected in the heart and lungs. Concentration in the spleen was undetected. The authors did not evaluate the concentration in the intestine.[26] These discrepancies could be attributed to variations in the routes of administration, diverse animal models, and the distinct forms of NIC (such as salt) utilized in the studies.

Additionally, Yang et al introduced a novel NIC prodrug (PDNIC).[30] Their research revealed that following both intravenous (IV) and oral (PO) administrations of PDNIC, there was a notably high tissue-to-plasma $AUC_{0-\infty}$ ratio in well-perfused tissues such as the heart, lung, kidney, liver, spleen, and intestine. Conversely, distribution to adipose tissue and the brain was comparatively lower.

NIC Modifications for Solubility Enhancement

NIC Derivatives

The literature reports various NIC derivatives and their superior biological activity. However, the main focus of this review will be the solubility and pharmacokinetic improvement of the new derivatives. Some of the derivatives with the most prominent improvement in solubility, biological activity and ADME (Absorption, Distributions, Metabolism, Excretion) characteristics are presented in Figures 1 and 2.

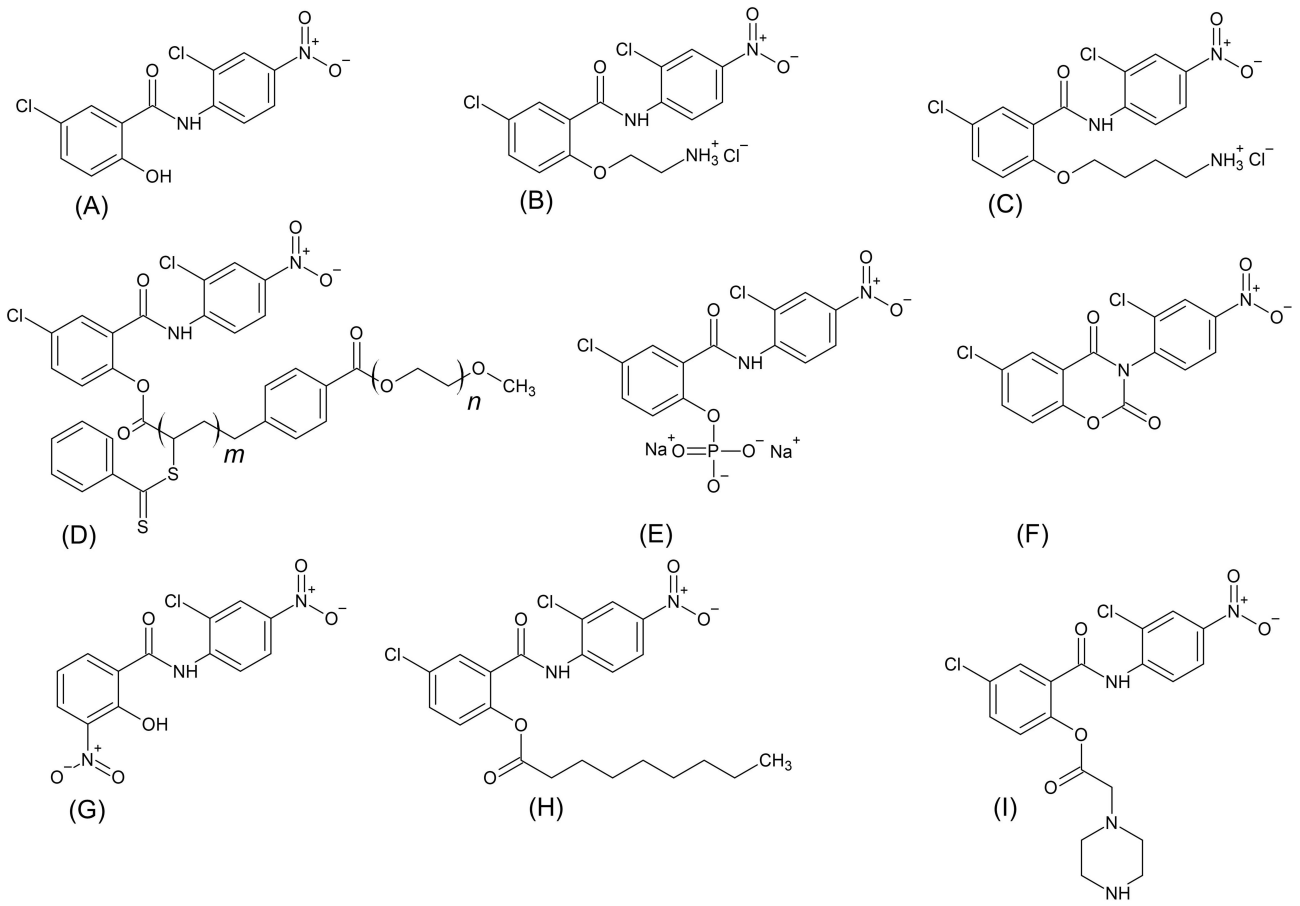

Figure 1 Chemical structure of NIC (**A**) and derivatives with enhanced solubility and biological activity prepared by Chen et al[31] (**B**), Xu et al[32] (**C**), Ma et al[33] (**D**), He et al[34] (**E**), Wu et al[35] (**F**), Li et al[36] (**G**), Mook et al[37] (**H**) and Yang et al[38](**I**).

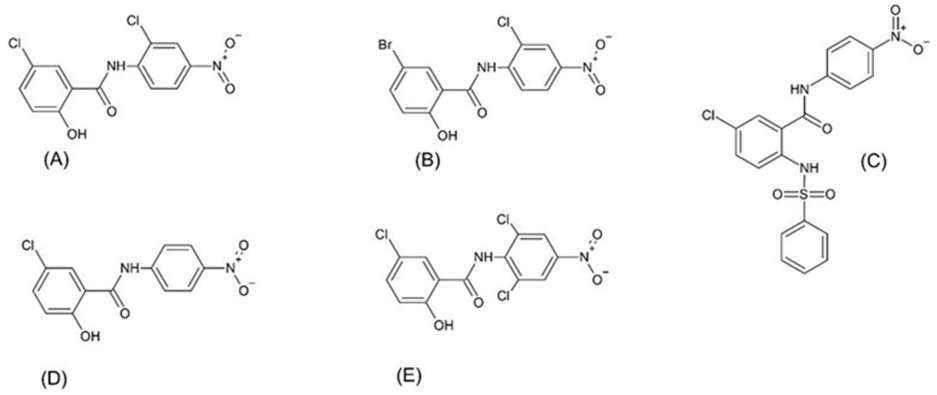

Figure 2 The chemical structure of NIC (**A**) and selected derivatives (**B-E**) synthesized by Shamim et al[38] that show activity against the SARS-CoV-2 infection and Zika virus with significantly improved in vitro drug-like properties such as microsomal stability, solubility, and PAMPA permeability compared to NIC.

Chen et al modified the hydroxyl group on the phenol ring of NIC, introducing an O-alkylamino side chain (Figure 1B).[31] The author stated that scaffolds containing amino groups are crucial motifs for structural tuning, possessing the capability to engage in hydrogen bonding, and are therefore expected to have better solubility. The most successful derivatives were produced through the Mitsunobu coupling of NIC with N-Boc-protected amino alcohols, followed by Boc deprotection. Compounds HJC0125 and HJC0152, among all derivatives, not only showed

improved anticancer activity but also displayed a notable increase in aqueous solubility. Indeed, compound HJC0125, with a pentylamine side chain, showed a saturated concentration of 248 μg/mL, indicating a 1080-fold improvement in water solubility. Compound HJC0152 with an ethylamine side chain, exhibited a saturated concentration of 762 μg/mL, improving water solubility of NIC by 3300-fold. Additionally, it was demonstrated that in MDA-MB-231 cells, the novel derivative HJC0152 suppressed STAT3 promoter activity, increased active caspase-3 expression, halted cell-cycle progression, and induced apoptosis. Furthermore, in nude mice presenting breast tumor xenografts, HJC0152 significantly inhibited the growth of MDA-MB-231 xenograft tumors in vivo.

Xu et al further synthesized O-alkylamino-tethered derivatives of NIC.[32] The most successful compound (HJC0431) with 4-aminobutyl moiety (Figure 1C), was also synthesized via the Mitsunobu coupling reaction, as described earlier. Compound HJC0431 revealed a saturated concentration of 650 μg/mL. In this study, aiming to develop novel antibacterial derivatives this compound also showed the broadest antibacterial activity, being effective against 6 strains.

The ethanolamine salt of NIC was also synthesized. It was reported that the solubility of ethanolamine salt increases to 180–280 mg/L at 20 °C compared to 5–8 mg/L of NIC and that this form of NIC has an excellent safety profile[8,39.] The synthesis of NIC ethanolamine salt (NEN) is reported by Kapale as by patent CN106496060A.[8] Tao et al discovered that NEN exhibits a remarkable antidiabetic effect in mice. Following oral administration, the LD_{50} value of NEN remained consistent or even higher compared to NIC. This observation indicates that pro-longed oral therapy with NEN does not present any toxic effects.[26] Ma et al synthesized pegylated NIC with mPEG-5000 (mPEG5000-nic, Figure 1D)) by reversible addition-fragmentation chain transfer polymerization (RAFT) method.[33] It was designed for injectable administration. The authors reported that the water solubility of the pegylated NIC was over 1.8 mg/mL, representing an 8000-fold increase with respect to pure NIC. The authors attributed the enhanced solubility to the self-assembly of mPEG5000-NIC in water. This self-assembly improved the water solubility of NIC, as the hydrophilic chain segment mPEG mutually entangled and enveloped the hydrophobic group NIC. Consequently, NIC was evenly distributed in the water without precipitation. The in vitro release experiment was conducted in phosphate-buffered saline (PBS) with a pH of 7.4 and a concentration of 0.01M, supplemented with 0.5% (wt/wt) Tween 80. NIC, grafted onto the copolymer, exhibited a gradual and sustained release extending up to 11 days, with cumulative drug release exceeding 80%. The novel formulation demonstrated antitumor efficacy both in vitro and in vivo, showing comparable antitumor activity to 5-fluorouracil but with lower toxicity.

In another investigation, He et al created a set of degradable NIC derivatives to target small-cell lung cancer.[34] The authors modified the hydroxyl group on the phenol ring of NIC, introducing a phosphate and disodium phosphate moiety (Figure 1E). The water solubility of the new derivatives was reported to be 7.2 mg/mL and 22.1 mg/mL respectively, while the water solubility of NIC was reported to be 0.06 mg/mL. This represents a 120-fold and 368-fold increase in aqueous solubility, respectively. These two compounds displayed anti-small cell lung cancer (SCLS) activity comparable to the most potent compound among the new derivatives, which had very limited solubility.

Wu et al synthesized a new NIC derivative, B17, obtained by the fusion of hydroxybenzamide NIC's ring (Figure 1F), targeting urological cancers.[35] The authors stated that B17 exhibited increased solubility (10.6 mg/mL) compared to NIC (1.6 mg/mL) in DMSO.

Another NIC derivative JMX0207, with a 3-NO_2 group, (without the 5-Cl moiety, Figure 1G) was tested in vivo and in vitro for antiviral efficacy against the Zika virus. The derivative showed improved pharmacokinetic properties. When given orally to B6 mice at a dose of 40 mg/kg, JMX0207 exhibited C_{max} of 145±18 μM (242-fold improvement), $T_{1/2}$ of 4.6±1.0 hours (2.39-fold increase) and an $AUC_{0-\infty}$ of 2719± 1018 (777-fold increase).[36]

Mook et al synthesized a series of NIC derivatives and discovered an acyl derivative, DK-520 (Figure 1H), which substantially increased both the plasma concentration and the duration of exposure to NIC when administered orally.[37] This results from the capacity of the derivative DK-520, which has a octanoyl moiety instead of the -OH, to metabolize into NIC, thereby increasing the exposure of NIC after oral administration. The derivatives were synthesized by coupling substituted anilines with 5-chloro-2-hydroxybenzoic acid. The authors reported that administering a 200 mg/kg solution of DK-520 to mice in corn oil resulted in higher plasma exposure compared to published studies on NIC orally dosed at 200 mg/kg, as referenced in the study by Osada et al[14] The C_{max}, AUC and the duration of exposure all increased with the new derivate. Plasma concentrations of NIC, following the administration of DK-520 at 200 mg/kg, surpassed the IC_{50}

for inhibiting Wnt signalling in the TOPFlash assay for nearly 24 hours. In comparison, the reported plasma levels of NIC dosed as a solution at 200 mg/kg were only above the IC_{50} for Wnt inhibition in the TOPFlash assay for less than 1 hour. Moreover, this elevated NIC exposure did not lead to any observed toxicity.

Yang et al introduced a novel NIC prodrug (PDNIC) called NCATS-SM4705 (Figure 1I).[30] The prodrug exhibits an acyloxy piperazine moiety on the -OH group. PDNIC exhibited a remarkable 40-fold increase in solubility at pH 7.4 when compared to NIC. The in vitro metabolic stability of PDNIC was assessed using plasma and liver fractions from mice, hamsters, and humans. PDNIC exhibited rapid biotransformation to NIC in mouse and hamster plasma, but a significantly slower biotransformation in human plasma. In mouse and human liver microsomes, only a minor fraction of PDNIC was converted to NIC, whereas a slightly higher proportion of NIC was converted to NIC in hamster microsomes. In vivo studies conducted in mice following both intravenous (IV) and oral (PO) administration demonstrated high oral absorption of PDNIC, with a bioavailability of 85.6% and a moderate clearance. The formulation used was composed as follows: 5% ethanol, 60% PEG-300 and 35% of 20% HP-β-CD solution in water. The administered doses were 3 and 10 mg/kg for IV and 10 mg/kg for PO gavage. The authors noted that PDNIC can be effectively converted to NIC in vivo following both intravenous (IV) and oral (PO) doses, with the plasma $AUC_{0\text{-}\infty}$ ratio of NIC to PDNIC ranging from 0.34 to 0.48. The dose-normalized $AUC_{0\text{-}\infty}$ of NIC was 216 (h*ng/mL)/(mg/kg) after a PO dose of PDNIC (10 mg/kg), which was 8-fold higher compared to a PO dose of NIC at 40 mg/kg as the authors compare to the study reported by Fan et al[22] As stated before, PDNIC was highly distributed in well-perfused tissues (heart, lungs, kidney, liver, spleen and intestine) and presented a low distribution in adipose and brain. The V_{dss} was 0.28–0.33L. Additionally, following an oral dose of 10 mg/kg PDNIC, the lung-to-plasma $AUC_{0\text{-last}}$ ratio of NIC was approximately 0.97, marking a 3.6-fold increase compared to 0.27 reported after an oral dose of NIC (40 mg/kg).[22] Following intravenous doses of PDNIC, the formed NIC exhibited a terminal half-life ($T_{1/2}$) ranging from 2.7 to 4.5 hours in plasma and similar half-lives in other tissues, except for the liver, where the elimination of NIC was notably 4-fold slower than in all other tissues, with terminal half-lives ranging from 11.6 to 21.2 hours. Similar profiles were observed in the 10 mg/kg oral group. In vivo studies were conducted in hamsters using both intravenous (IV) and oral (PO) doses. The IV dose administered was 3 mg/kg, while the PO dose was 30 mg/kg. The formulation used for both IV and PO administration was 20% HP-β-CD in water (0.6 mg/mL for IV and 3 mg/kg for PO). PDNIC demonstrated efficient conversion to NIC in vivo, with plasma $AUC_{0\text{-}\infty}$ ratios (NIC/PDNIC) of 0.32 and 0.44 after both IV and PO doses, showing similarity to observations in mice. The dose-normalized $AUC_{0\text{-}\infty}$ of NIC was 88 (h*ng/mL)/(mg/kg) after the PO dose of PDNIC (30 mg/kg), slightly lower than that observed in mice. The prodrug exhibited a V_{dss} of 0.74 L in hamsters. Additionally, after both IV and PO doses of PDNIC, the lung to plasma $AUC_{0\text{-}\infty}$ ratio of NIC was 72 and 107 respectively. This value is quite higher than that in mice. Following an oral dose of 30 mg/kg, the bioavailability of PDNIC in hamsters is approximately 64%, slightly lower than that observed in mice. It's worth mentioning that the formulation media for mice and hamsters differed. The mice formulation contained 60% PEG-300. This raises questions about whether PEG might impact the formulation outcome in some way and be also responsible for some differences in pharmacokinetic parameters.

Shamin et al synthesized a series of NIC derivatives (Figure 2), concentrating on the anilide and salicylic regions of NIC to enhance physicochemical properties and target the inhibition of Zika virus and SARS-CoV-2 infection.[38] The objective was to investigate the impact of electron-donating and electron-withdrawing substitutions in both regions of NIC. The authors aimed to identify a suitable replacement for the aniline 4-NO_2 group, which could undergo reduction and glucuronidation in vivo. Among all tested compounds, the 5-bromo substitution in the salicylic acid region demonstrated retained potency along with improved ADME properties. It exhibited enhanced solubility (8 µg/mL), good rat liver microsomal stability ($t_{1/2}$ greater than 30 min), and increased PAMPA permeability (6.7 x 10^{-5} cm/s). Moreover, the alterations in the anilide region with 2-OMe and 2-H substitutions demonstrated comparable IC_{50} values to NIC in the NS-1 assay, while exhibiting markedly improved physicochemical properties compared to NIC. Through modifications in the anilide region, it was discovered that 4-CN and 4-CF_3 served as suitable replacements for 4-NO_2. These compounds exhibited similar potencies to NIC in the NS-1 inhibition assay while offering enhanced physicochemical properties, such as microsomal stability, solubility, and PAMPA permeability.[38]

Amorphous Solid Dispersions

The use of hydrophilic polymers in creating amorphous solid dispersions (ASDs) is a well-established method to enhance the aqueous solubility of poorly soluble drugs, directly impacting bioavailability.[40] ASDs, generally, are dispersions where the drug is dissolved within a solid matrix, typically a polymer.[41] Amorphous materials enhance the apparent solubility of the drug by increasing its thermodynamic activity when it is dispersed in a molecularly and randomly distributed manner within the polymer.[42,43] NIC has a limited ability to form an amorphous solid on its own, as it is a poor glass former with a high tendency to recrystallize. However, it can form an amorphous solid dispersion (ASD) when dissolved in a solid matrix, such as a polymer.[2] Furthermore, the addition of a third component (surfactant, polymer, or excipient) prevents drug precipitation and stability issues, offering advantages like controlled drug release, heightened drug loading, and improved stability compared to binary ASDs.[40] Jara et al developed an amorphous solid dispersion (ASD) of NIC that generates nanoparticles during dissolution.[1] It was prepared by the hot melt extrusion method wherein the drug was formulated with poly (1-vinyl pyrrolidone-co-vinyl acetate (PVA-VA). The NIC ASD produced nanoparticles with an average particle size of approximately 100 nm in fasted simulated intestinal fluid (FaSSIF) media. The ASD not only raised NIC apparent solubility from 6.6±0.4 to 481.7 ± 22.2 µg/mL in FaSSIF, representing a 60-fold increase but also enhanced its oral availability by 2.6 times in Sprague-Dawley rats when administered as a suspension. The same formulation was also administered as capsules containing sodium bicarbonate to counteract the acidic stomach pH, but, there was no statistically significant increase in bioavailability. Furthermore, in a side-by-side diffusion test, where the media was FaSSIF and decanol, a four-fold increase in NIC diffusion was reported. However, the same authors stated that NIC ASD in acidic media, undergoes recrystallization, suggesting that an enteric coating would be necessary to avoid this problem. In a further study of the same group, the overall formulation contained NaCl to facilitate the dissolution of the tablets, croscarmellose sodium as a disintegrant, and microcrystalline cellulose, and was sealed with the poly(vinyl alcohol)-based coating known as Opadry® II Clear.[9] After that, the tablets were enteric coated with Acryl-EZE® 93 A. The enteric-coated tablets were administered to fasted beagle dogs. The administration dose was 75 mg/kg. The detected plasma concentrations were up to 149 ± 79.2 ng/mL. The plasma concentrations achieved were superior to those documented with NIC dissolved in a blend of solvents, polymers, and pH modifiers (DMSO, PEG, NaOH, and saline buffer) given at a higher dose (100 mg/kg) to beagle dogs.[23] This proves the success of the enteric coat in protecting the formulation from the acidic environment.

Bhanushali et al developed a variety of binary and ternary amorphous solid dispersions of NIC with various polymers and polymer to NIC ratios.[40] The most successful was the one containing NIC and hydroxyethyl cellulose (HEC) in a NIC-to-polymer ratio of 1:4. The p-XRD findings confirmed the amorphous trans-formation of NIC within the formulation. The water solubility of NIC increased significantly by 70 times (428.333±14.142 µg/mL) compared to pure NIC (6.14 ± 0.67 µg/mL). The pharmacokinetics of NIC and the ASD formulation of NIC were compared in healthy female Wistar rats at a dose of 25 mg/kg administered orally. The authors reported a 4-fold improvement in C_{max}. The $AUC_{0\text{-}t}$ presented a 4.41-fold increase while the $AUC_{0\text{-}\infty}$ presented a 4.17-fold increase.

NIC Co-Crystals

Co-crystal engineering provides an alternative approach to modify the physicochemical properties of a drug, thereby enhancing drug delivery. Co-crystals consist of two components with a fixed stoichiometric ratio, connected by non-covalent bonds. One component is the pharmaceutically active drug, and the other is the inactive co-former, typically considered a Generally Recognized as Safe (GRAS) molecule.[44] Co-crystals are documented to effectively improve the solubility, dissolution rate, bioavailability, and physical stability of active pharmaceutical biomaterials.[45]

Ray et al developed an inhalable co-crystal formulation of NIC-nicotinamide (NIC-NCT) via a rapid and continuous spray drying method (SDC) and a solvent evaporation method (SEC) for comparison.[44] Needle-shaped co-crystals with a mean particle size of 11.52 ±6.65 µm were obtained from the solvent evaporation method. In contrast, spherical co-crystals, with a mean particle size of 4.76 ±1.26 µm were obtained by the spray drying method. The yields for NIC-NCT co-crystals, produced via spray drying and solvent evaporation methods, were 71.4% ± 8.46% and 66.4% ± 7.33%, respectively. DSC analysis indicated that a glassy transition was observed in the case of spray-dried NIC-NCT co-crystal powder. Such transitions are primarily characteristic of amorphous powders. The co-crystals of the drug exhibited

a substantial improvement in solubility. Furthermore, SEC NIC-NCT co-crystals showed a 5.9-fold increase, while SDC NIC-NCT demonstrated a 14.8-fold increase in the dissolution of NIC. Furthermore, SDC improved aerodynamic parameters, including MMAD (median mass aerodynamic diameter) and FPF (fine particle fraction), enhancing its suitability for inhalation and deposition within the deep lung. In contrast, needle-shaped SEC co-crystals exhibited a larger mass median aerodynamic diameter size and lower fine particle fraction compared to spherical SDC. These findings suggest the inadequacy of the SEC formulation for in vitro inhalation. Moreover, SDC demonstrated higher anti-proliferative activity against human lung adenoma cells in a dose-dependent manner, surpassing both NIC alone and SEC co-crystals. However, the poor glass-forming ability of NIC demonstrated previously[1] may lead to physical instability of the spray-dried system. In this light, the recrystallisation of amorphous NIC-NCT spray-dried product should be further examined.

Ludeker et al employed solvent-assisted solid grinding and/or slow solvent evaporation to produce new co-crystals of NIC.[46] NIC-aminothiazole 1:1 co-crystal (NIC-AT) proved to be the most successful among them. The other candidates were NIC-benzamide, NIC-isoniazide and NIC-acetamide. The equilibrium solubility of NIC-AT co-crystals was reported to be 2.8 times higher than that of NIC. Furthermore, the newly developed NIC-AT co-crystal exhibits notable stability, lasting for over 18 months, likely attributed to its robust hydrogen bonding motifs.

Grifasi et al obtained a new series of salt co-crystals by grinding NIC with carbonates and bicarbonates. Additionally, a mechanochemical reaction with imidazole yielded a classical co-crystal. Furthermore, two new salts were generated via the salification of NIC with NaOH and subsequent kneading with DMSO.[47] According to the authors, a "salt co-crystal" refers to the concurrent existence of a neutral molecule and its salt within the same unit cell, engaging in hydrogen bonding interactions. The dissolution tests were conducted in an ethanolic aqueous solution (1:1). The most soluble sample was found to be 'NaNIC·HNIC·$2H_2O$', which was synthesised by kneading (absolute ethanol) NIC with sodium carbonate, in a 4:1 stoichiometric ratio, at room temperature for 35 minutes. The intrinsic dissolution rate of NaNIC·HNIC·$2H_2O$ increased by a factor of 5. The concentration of NIC after 72 hours has been reported as 24 mg/L for the NaNIC·HNIC·$2H_2O$ and 3.5 mg/L for pure NIC.

Sanphui et al prepared 1:1 co-crystals of NIC with caffeine, urea, p-aminobenzoic acid, theophylline, nicotinamide, and isonicotinamide.[48] The preparation of NIC co-crystals was achieved through dry grinding, wet granulation, and slow evaporation methods. Dry solvents (ethyl acetate and acetonitrile) were used to avoid hydrate formation. NIC-theophylline acetonitrile solvate (NIC-THPHS) showed the highest solubility in 40% i-PrOH-water after 24 h, followed by NIC theophylline co-crystals (NIC-THPH). The improvements in solubility were 1.4- and 1.31-fold respectively. Powder dissolution in the same medium was carried out and after 2 hours, NIC-THPHS showed the fastest dissolution rate (6.3-fold increase) followed by NIC-THPT (5.1-fold increase). The authors noted that all crystalline forms transformed into NIC mono-hydrate (H_A) within 24 hours, leading to a very similar solubility for all co-crystals.

In a recent paper, D'Abbrunzo et al prepared the novel NIC co-crystal by combining it with praziquantel (PZQ), another anthelminthic drug.[49] Such dual-drug antiparasitic co-crystals were obtained through a sustainable one-step mechanochemical process by grinding a PZQ/NIC molar ratio of 1:3 in the presence of micromolar amounts of methanol for 120 min at 25 Hz, resulting in pure solid products, without any traces of the starting reagents or solvent. Also, both drugs retained their chemical stability during the grinding procedure, regardless of the typical tendency of PZQ to degrade during the grinding. The novel solid phase crystallizes in the monoclinic space group of P21/c, showing one PZQ and three NCM molecules linked through homo- and heteromolecular hydrogen bonds in the asymmetric unit, showing a plate-like habitus ranging in size from 150 to 15000 nm. PZQ/NIC co-crystal presented a melting point of 202.89°C, which is intermediate to those of the parent compounds (ie 141.9 and 229.98°C for PZQ and NIC, respectively). The supramolecular interactions confer favorable properties to the co-crystal, preventing NIC transformation into the insoluble monohydrate both in the solid state and in the aqueous solution. After 72 h of exposure, PZQ/NIC co-crystal exhibits higher anthelmintic activity against adult *Schistosoma mansoni* in vitro than the corresponding physical mixture of the APIs (IC_{50} 0.02123 and 0.09610 μM, respectively) Such prominent efficiency of PZQ/NIC co-crystals was further confirmed on the mice models with chronic *S. mansoni* infection.

Nano-Based Drug Delivery Systems

Nanosized materials possess unique physicochemical properties, featuring a significant surface area-to-mass ratio and enhanced permeability and solubility. These characteristics offer potential solutions to the limitations of traditional therapeutic and diagnostic agents.[50] Heightened surface area improves particle adhesion to biological membranes, enhancing cellular uptake. Drug incorporation into nanocarriers helps reduce degradation and toxicity. Nanomaterials play a crucial role in drug targeting, where nanocarrier surfaces can be coated with ligands binding to receptors overexpressed by target cells, like in cancer disease.[10] Despite the numerous advantageous features of nanocarriers, a primary drawback or challenge is their stability. These systems exhibit high total surface energy, rendering them thermodynamically unstable and prone to agglomeration, resulting in an increase in particle size. Hence, the utilization of polymers and/or surfactants are commonly employed strategies to maintain the stability of the system.[10] Various strategies have been employed to develop nanostructured systems, as listed below.

Nanocrystals

Drug nanocrystals, are created by reducing the particle size of the micronized compound to the nanoscale. These colloidal dispersion systems are stabilized in water using surfactants or polymers.[10,25] One advantageous aspect of nanocrystals is that the formulation does not necessitate the incorporation of the drug into a matrix system, allowing for 100% drug loading in the nanoparticles.[10] Drug nanocrystals represent an intermediate stage in the preparation process, adaptable for further formulation into tablets, capsules, sprays, injections, and various administration routes.[25]

Ye et al formulated an injectable nanocrystal formulation of NIC was developed using a top-down wet milling technique.[25] Tween 80 was chosen as a stabilizer. The final formulation comprised one aliquot of Tween 80 and five aliquots of NIC. The obtained nanocrystals had a mean particle size of 235.6 nm with a unimodal distribution. The nanocrystal formulation exhibited no significant difference in the drug release profile, as determined by the reverse bulk equilibrium method using a pH 7.4 buffer with 0.2% Tween-80 as the medium. Sprague-Dawley rats were administered a NIC-nanocrystal suspension or a NIC solution (dissolved in 30% alcohol/45% PEG400/20% water) through the jugular vein at a dose of 2 mg/kg. The newly formulated product did not demonstrate a significant enhancement in the plasma concentration versus time profile when compared to pure NIC. The authors postulated that the rapid release of drug molecules into the bloodstream upon intravenous administration could be a contributing factor. However, there was a significant difference in the biodistribution. The nanocrystal formulation exhibited higher drug levels in the heart, spleen, and lungs after 4 hours, indicating ongoing distribution at that time point. The most significant difference was observed at 2 hours, with NIC solution showing higher tissue drug levels than the nanocrystal formulation, in all tissues, implying longer blood residence time for NIC nanocrystals. The physical and chemical stability of the NIC nanocrystals was satisfactory after 60 days of storage.

Lin et al utilized the electrospray technique to create NIC nanoparticles for assessing their anticancer activity against ovarian cancer cells.[50] The nanosuspension included 1% polyvinyl alcohol (PVA) in a phosphate-buffered saline solution. The average particle diameter was 105 nm. The dosing solution, formed by dissolving nano-NIC in PBS, was orally administered or intravenously (IV) injected to female Sprague-Dawley rats at doses of 5 mg/kg and 2 mg/kg, respectively. The *AUC* was calculated to be 669.5 and 1058 h(ng·mL) for the oral and IV routes, respectively. The estimated oral bioavailability was 25%, surpassing the reported 10% bioavailability of NIC. The authors noted a swift rise in NIC plasma concentration for both oral and IV routes, followed by a rebound peak at 4 hours. Since the second peak was also observed for the IV route, the authors attributed this phenomenon to an enterohepatic recycling mechanism. They mentioned that this observation aligns with the findings of a prior study in mice[14]. The nanosuspension effectively inhibited the metabolism and in vitro growth of CP70 and SKOV3 cells, achieving IC_{50} values of 3.59μM and 3.38 μM, respectively.

Bai et al also developed novel NIC suspensions using a single- or dual-capillary electrospray system (ES) addressed in ovarian cancer treatment, in vitro.[51] The ES technique is employed to reduce the size of raw NIC powder particles (Nano-NIC), which are subsequently suspended in PBS containing a stabilizer. Homogeneous suspensions of pure NIC or NIC-encapsulated poly (D, L-lactic-co-glycolide) (PLGA) particles were developed. The single- or dual-capillary ES

system offers versatile fabrication, enabling control over drug carrier configurations, including nanocrystalline, matrix type, or core-shell type. This is exemplified by the creation of Matrix-type NIC-PLGA and core-shell type NIC-PLGA nanoparticles using single- and dual-capillary electrospray (ES), respectively. The suggested electrospray (ES) was operated in a cone-jet mode to generate particles of NIC, with or without a PLGA shell that can be readily suspended in a water-based solution to form a suspension. This strategy minimizes the utilization and remnants of organic solvents in drug formulation. Pure NIC nanoparticles were rod-shaped (105 nm x 493 nm), while NIC-encapsulated PLGA particles are spherical, with a diameter of approximately 584–662 nm. Nano-NIC particles, without PLGA encapsulation, release NIC faster than PLGA-encapsulated particles and raw NIC powder within 500 hours. They show approximately 1.6-fold increased water solubility compared to raw NIC, possibly due to enhanced surface area. Nano-NIC particles released 31.6%, compared to raw NIC powder which released 19% of the total amount of NIC within 500 hours of test time. Interestingly, the core-shell NIC-PLGA nanoparticles displayed a two-stage release profile, while the matrix NIC-PLGA nanoparticles exhibited a faster and gradually elevated release over the 500-hour test. Beyond 500 hours, the release kinetics of NIC-PLGA particles accelerate more than nano-NIC particles. This is believed to be due to the degradation of PLGA, leading to the abrupt release of embedded NIC molecules. The authors suggested, according to Sardo et al[52] that reducing particle size would be advantageous, as the release kinetics of drug-encapsulated PLGA particles are closely tied to their particle size. Nano-NIC and NIC-PLGA suspensions showed a stronger anti-proliferative ability than the conventional NIC. The matrix NIC-PLGA nanoparticles exhibited an IC_{50} of 1.37 µM in the treatment of CP70 cells. It is important to mention that the generated NIC (pure or encapsulated) was present as a monohydrate and not as an anhydrous form.

Costabile et al developed an inhalable formulation of NIC through nanosuspension technology for the therapy of *Pseudomonas aeruginosa*.[53] The group created dry powders containing NIC nanoparticles, which can be reconstituted in saline solution to produce inhalable nanosuspensions. NIC nanoparticles were generated through high-pressure homogenization (HPH), with polysorbates employed as stabilizers. Following 20 cycles of HPH, all formulations exhibited comparable characteristics, appearing as needle-shaped nanocrystals with a hydrodynamic diameter of around 450 nm. The nanosuspensions stabilized with 10% w/w polysorbate 80 to NIC (T80_10) displayed an optimal solubility profile in interstitial lung fluid. T80_10 was effectively converted into a mannitol-based dry powder using the spray-drying technique. (T80_10 DP). Dry powder was reconstituted in saline solution. The results from in vitro release studies of NIC, conducted using a dialysis membrane from simulated cystic fibrosis (CF) mucus to simulated interstitial lung fluid (SILF), indicated no significant difference in the percentage of NIC diffused after 8 hours between T80_10 DP (58.1 ± 6.5%) and T80_10 (63.3 ± 8.0%). Conversely, the diffusion rate of Micro NIC (raw NIC micronized through a colloidal mill) considerably slowed down (22.9 ± 1.3%). The reconstituted spray-dried particles in saline solution were efficiently delivered via commonly used nebulizers, with optimal performance observed using the PARI TurboBOY and Aeroneb Pro nebulizers. The nanosuspensions demonstrated in vitro quorum sensing inhibition of *P. aeruginosa* at non-toxic concentrations for CF bronchial cells. In vivo data affirmed the absence of acute toxicity at therapeutic doses. Despite these positive results, Brunaugh et al[54] noted that the amount of polysorbate used exceeds what is currently FDA-approved for inhaled products. Furthermore, they pointed out that the utilization of mannitol as the carrier system may induce bronchospasm and cough.[54]

Furthermore, Hobson et al developed a long-acting injectable solid dispersible nanoparticulate formulation (SDN) for the treatment of Covid-19, intended for intramuscular administration.[55] The advantage of SDNs lies in their composition, consisting solely of the active pharmaceutical ingredient (API), and their ability to be stored in solid form, and then easily re-dispersed in water before use. Briefly, this formulation was obtained by inducing nanoprecipitation of NIC when NIC is pumped into an aqueous solution of stabilizers (HPMC) and sugars (sucrose), sonicating the dispersion and pumping it into a spray-dryer. The obtained nanoparticles can be dispersed in aqueous media for injection. The sustained-release characteristics of NIC delivery via nanoprecipitation were assessed in vivo over 28 days in Sprague Dawley rats. Three distinct intramuscular doses: 50, 100, and 200 mg/kg were administered. All injected doses achieved a maximum concentration (C_{max}) within 3 hours. The bioavailability increased with higher doses. The C_{max} values were reported to be 1408.6, 2041.3, 3125.3 ng/mL and *AUC* of 28955, 55,734, 74584 ng h /mL for 50, 100, and 200 mg/kg doses. A sustained plasma exposure was unmistakably attained, and the release kinetics were characterized as "flip-flop." As

stated by the authors, his phenomenon is particularly beneficial for long-acting therapeutics, as it often occurs when drug absorption from extravascular routes appears slower than the rate of drug elimination. Furthermore, the authors reported that no obvious local toxicity was observed during the 28 days of the in vivo study.

Micelles

Polymeric micelles have demonstrated the ability to enhance drug solubility and reduce toxicities when compared to traditional carriers.[56] These micelles comprise hydrophilic and hydrophobic chain segments, forming core-shell nano-micelles with an inner lipophilic and outer hydrophilic structure.[57] Hang et al prepared micelles named PEG2K-FIbu/NIC by a thin film dispersion method. They incorporate a hydrophilic PEG chain segment, a Fmoc motif, and the hydrophobic structural domain of ibuprofen while encapsulating NIC.[57] Ibuprofen was chosen for its ability to enhance the stability of micelles. The particle size of PEG2K-FIbu was 11.11 nm while the encapsulation rate was 70.4% The tumor inhibition rate was 55.98%.

Bhattacharyya et al developed a formulation in which NIC is covalently conjugated to a genetically-encoded elastin-based chimeric polypeptide (CP).[58] This CP comprises an elastin-like polypeptide, a disordered and highly water-soluble recombinant peptide polymer, fused to a short peptide segment containing thiol-reactive sites for the chemical conjugation of chemotherapeutic drugs. The resulting prodrug spontaneously self-assembles into 100 nm near-monodisperse micelles. The new formulation increased NIC half-life to 4.2 hours from 1 h. CP-NIC dissolved in PBS was injected in CD1 mice vein at a dose of 128 mg/kg. The plasma *AUC* of the CP-NIC was 36.9 ± 7.34 µg/mL/h compared to 3.3±1.3 µg/mL/h of unconjugated NIC. The plasma levels of CP-NIC at the dose of 128 mg/kg body weight stayed above the IC_{50} of Wnt signaling inhibition by NIC in the TOPFlash assay for nearly 24 hours, whereas unconjugated NIC remained above the IC_{50} for less than 1 hour. Unfortunately, the new conjugate expressed a low drug loading of 2% NIC only.

Russo et al designed biotin-targeted Pluronic P123/F127 mixed micelles (PMM) delivering NIC via intravenous injection to treat drug-resistant lung cancer cells.[6] Pluronic F127 was biotin-conjugated for tumour targeting, and Pluronic 123 was labelled with rhodamine B for fluorescence tracking of micelles in a biological environment. NIC was encapsulated in the PMM. Approximately 8.3% of the micelle surface was covered with biotin. The Biotin-PMM were almost spherical in shape with a diameter in the range of 25–35 nm. The optimal formulation condition for NIC encapsulation was at 40 mg/mL for the Pluronic mixture and 0.7 mg/mL for NIC. The release profile of NIC from NIC-loaded Bio-PMM in phosphate-buffered saline (PBS) at pH 7.4 was assessed using the dialysis method. NIC demonstrated a biphasic release profile, with an initial burst (first 6 hours) followed by a sustained release phase lasting up to 48 hours. In Dulbecco's modified Eagle's medium (DMEM) supplemented with 10% fetal bovine serum (FBS), the release profile followed a biphasic pattern again, occurring at a slower rate, lasting up to approximately 75 hours. The results showed an increased presence of biotin-decorated PMM in cancer cells compared to normal cells. The enhanced cytotoxicity of biotin-targeted micelles loaded with NIC was clearly observed in A549 cells resistant to cisplatin and 5-FU.

Misra et al innovated the "niclocelle" by integrating NIC into well-defined rigid core polymeric micelles using a solvent evaporation method, following a mixed micellar approach.[59] A tetrahydrofuran (THF) solution containing amphiphilic diblock co-polymer (polystyrene-block-polyacrylic acid) and a micellar suspension of polyethylene glycol cetyl ether (PEGCE) were co-self-assembled, incorporating NIC in the process. Control particles, called nanocelles are rigid core mixed micelles, without the inclusion of NIC, prepared with the same procedure. Incorporating PEGCE is crucial for limiting particle size to below 100 nm and enhancing micellar stability. The nanocelles had a size of approximately 100 nm, whereas the niclocells measured around 60 nm. This size reduction is likely attributed to the T-T interactions occurring between the aromatic moieties of the outer shell and NIC. The findings revealed an 87% loading of NIC in niclocelles. The drug release profile, in Dulbecco's Phosphate-Buffered Saline (DPBS) at pH 7.4, showed an initial release of approximately 41% within the first 12 hours, followed by sustained release leading to a total release of about 82% over the 96-hour observation period. A significant enhancement in IC_{50} values ranging from 2.5- to 4-fold was observed for niclocelle compared to NIC across MCF-7, MDA-MB231, and MCF-7 cells.

Nanohybrids

Nanohybrids consist of composite or hybrid materials comprising two or more components, with at least one component existing at the nanoscale.[60] The favorable properties and promising biomedical applications of organic/inorganic nanohybrids have garnered significant attention. Considerable efforts have been devoted to creating adaptable nanohybrids, with a variety of polymers emerging as notable organic components among them. These polymers provide distinct pathways for creating multifunctional systems with collective properties.[61] In the domain of inorganic nanomaterials, clay-based nanoparticles, particularly layered double hydroxide (LDH) and montmorillonite (MMT), have received considerable attention for their applications in nanomedicine. Additionally, a variation of LDH known as hydrotalcite (HT) has been found to possess biocompatibility and mucoadhesive properties.[62] Enhancing the dissolution of poorly soluble drugs through drug adsorption on silica materials represents a feasible and appealing strategy. This is attributed to several factors, including the substantial surface area, adjustable pore volume, controllable structural and textural parameters, and the abundance of silanol groups on the surface, which serve as potential sites for functionalization.[11]

Pardhi et al developed a mesoporous drug delivery system where NIC was loaded on silica carriers by the solvent evaporation method.[11] Carriers with a pore size of 2–37 nm, pore volume of 0.4–1.8 cm^3/g, particle size of 0.012–150 µm, and specific surface area of 40–1000m^2/g were selected for the study. The authors developed a discriminatory dissolution medium to perform the in vitro dissolution of NIC. This consisted of the addition of 2% Tween 80 to a pH 7.4 buffer. Despite higher drug loading observed at a 1:1 ratio of drug to carrier, the drug release was found to be greater at a 1:2 ratio compared to the 1:1 ratio. The authors elucidated this discrepancy by suggesting that at a 1:2 ratio, a monolayer of the drug could have formed within the pores of the mesoporous carriers. This process likely aided in retaining the drug inside the pores in its amorphous state, which, upon contact with the dissolution medium, could dissolve readily, leading to improved drug release. In contrast, at a 1:1 ratio, the potential deposition of multiple layers of drug inside and outside the pores could have led to drug crystallization on the surface of the mesoporous carriers, resulting in poor release. Around 37% of the plain drug dis-solved within 420 minutes. In contrast, all drug-loaded mesoporous carriers (at a 1:2 ratio) exhibited substantial enhancements in % drug release. Among these, Sylysia-350 demonstrated the highest drug release, achieving 100% release within 420 minutes. An initial burst release was observed, attributed to the drug's release from the surface. The carriers with larger pore sizes demonstrated the most favorable release profiles, while the microenvironmental pH, reflecting the pH on the excipient surface, also played a crucial role. Carriers with a basic microenvironmental pH exhibited superior release profiles, favoring the ionization of the drug. The cytotoxicity of the optimized mesoporous formulations of NIC was investigated in HCT-116, HCT-15, NCI, MDA-MB-231, and A549 cancer cell lines. Comparatively, a nearly three-fold increase in % cytotoxicity was noted for drug-loaded Syloid-244, and a two-fold increase for Sylysia 350 at a 1:2 ratio, compared to the plain drug.

Piao et al proposed an oral formulation comprised of three different mesoporous silica biomaterials like MCM-41 (Mobil Composition of Matter No.14), SBA-15 (Santa Barbara Amorphous-15), and geopolymer encapsulated with NIC and coated with Tween 60 for the treatment of Covid-19.[63] MCM-41 and SBA-15 were chosen as drug carriers due to their ordered hexagonal structures, large surface areas, and pore volumes. The geopolymer (PG) was created using clay (ie kaolin) dissolved in an aqueous alkali solution. This PG adopts an MCM-41 structure, where some tetrahedrally coordinated Si (IV) atoms are replaced by Al (III) atoms, resulting in a negative charge within the pore. Alkali ions like Na^+ are stabilized within the pore to meet the charge neutrality criteria. With Na^+ present in the mesopores of PG with an MCM-41 structure, NIC can be encapsulated within the pores via ion-dipole interaction and released in a controlled manner by modifying the pore charge. Consequently, PG is anticipated to enable high NIC loading and enhance NIC solubility. NIC was loaded into the PG and other carriers via the solvent evaporation method (referring to NIC-PG, NIC-MCM-41, NIC-SBA-15). The particle size of NIC-PG, NIC-MCM-41, and NIC-SBA-15 were determined to be 616 ± 94, 719 ± 32, and 745 ± 74 nm respectively. In vitro NIC release from the nanohybrids was tested in simulated gastric (pH 1.2) and intestinal fluids (pH 6.8), containing 2% Tween 60. Nanohybrids notably enhanced NIC release compared to intact NIC, with a dual-phase release pattern: rapid initial release followed by sustained release. The nanohybrids displayed an initial release of 25% (NIC-PG), 28% (NIC-MCM-41), and 30% (NIC-SBA-15) within the first 10 minutes, with a cumulative release of more than 97% in 24h. The authors attributed the slower release of the NIC-PG nanohybrid to stronger ion-dipole interactions between Na^+ and NIC. Sprague-Dawley rats weighing 300 g were orally administered

50 mg/kg NIC of the Tween 60-coated nanohybrids. All three nanohybrids exhibited significant enhancement compared to intact NIC. The C_{max} of NIC-MCM-41 (284.75± 46.38 ng/mL) was roughly 1.8 times higher than that of NIC-PG (159.38±47.07 ng/mL) and NIC-SBA-15 (166.99±37.65 ng/mL). Moreover, the $t_{1/2}$ of NIC-SBA-15 (7.56 ±3.29 h) was approximately 1.8 times longer than that of NIC-PG (4.10±0.5h) and NIC-MCM-41 (4.54 ±0.67h). Regarding T_{max}, NIC-PG (2.67±1.15h) exhibited a T_{max} approximately 10.7 times higher than NIC-MCM-41 (0.25 ±0.0h) and NIC-SBA-15 (0.25 ±0.0h). Again, the highly improved T_{max} was attributed to the stronger ion-dipole interaction within the nanohybrid. The authors suggested that by regulating the pore size and charge density within the internal pores of silica nanohybrids, one could attain the desired drug release profile. Consequently, the overall release kinetics could be adjusted to achieve optimal outcomes.

Yu et al introduced an innovative hybrid drug delivery system comprising NIC, montmorillonite (MMT), and Tween 60 for the treatment of Covid-19.[7] NIC molecules were incorporated into the interlayer space of cationic clay, MMT, forming NIC-MMT hybrids, which were subsequently surface-coated with Tween 60. The hybrids were synthesized using a mechano-chemical method. A mixture of sodium MMT and NIC powders was ground in a mortar for 1 hour without solvent to prepare NIC (1.0)-MMT. Then, 26 mL of EtOH (99.9%) was added to prepare NIC (1.0)-MMT-E and. The molar ratio between NIC and MMT was 1.0:1.0, 1.0:1.0, and 1.3:1.0 respectively. Subsequently, Tween 60 was dissolved (NIC-MMT hybrids: Tween 60 = 3:2 w/w). The suspensions were dried using a rotary evaporator to obtain powder samples. The particle size of the hybrids was 550 ±87 nm for NIC (1.0)-MMT, 448 ±44 nm for NIC (1.0)-MMT-E, and 545±48 nm for NIC (1.3)-MMT-E. In vitro release studies were performed at pH 1.2 and 6.8. Under gastric conditions, only 8% of intact NIC dissolved after 2 hours. However, nanohybrids showed significantly enhanced release. NIC (1.3)-MMT-E had the highest release, reaching 55% within 0.5 hours, possibly due to NIC molecules adsorbed on the MMT carrier's external surface. Under intestinal conditions (pH 6.8), NIC exhibited a slight increase in solubility (15%) during the first 2 hours due to the higher pH. NIC (1.3)-MMT hybrid released NIC very rapidly (75% within the first 10 minutes), likely due to NIC molecules present on the external surface. In contrast, NIC was released steadily for up to 10 hours for NIC (1.0)-MMT and NIC (1.0)-MMT-E. Male Sprague-Dawley rats were fasted overnight and were orally administered with Yomesan® (the commercially available form of NIC) or Tween 60-coated NIC-MMT at a dose of 50 mg NIC/kg. The highest NIC levels were found in the rat plasma administered with Tween 60-coated NIC (1.0)-MMT-E, with C_{max} being 2-fold, AUC_{last}, 1.6-fold, and $AUC_{0-\infty}$ 1.5-fold higher compared to Yomesan®.

Rejinold et al developed NIC-loaded Zein nanoparticles which were coated with bovine serum albumin (BSA) as an injectable therapy against Covid-19.[64] It is noteworthy that BSA-based nano-biomaterials have been extensively studied in the drug delivery field, primarily due to their ability to specifically target infected sites.[65] The negatively charged NIC molecules in solution can interact electrostatically with the positively charged Zein, resulting in the formation of robust drug-loaded nanoparticles (NPs). The particle size of the BSA-Zein-NIC was determined to be 207±3.6 nm, manifesting a spherical morphology. Release studies at pH 7.4 revealed a maximum of 60% NIC release in the serum-containing buffer, which closely resembled NIC release in the serum-untreated buffer of the BSA-Zein-NIC NPs. This observation is logical, given the inherent serum coating on the BSA-Zein-NIC NPs. After 24 hours, NIC release reached saturation and subsequently decreased. The authors attributed the significantly improved release from BSA-Zein-NIC NPs to the enhanced solubility conferred by the BSA coating. Additionally, Zein's ability to swell in an aqueous medium further improves NIC release from the nanohybrid matrix.

Rejinold et al further developed a NIC-bovine serum albumin nanoparticle coated with polyethene glycol (BSA-NIC-PEG NPs) as an injectable treatment for Covid-19.[66] The particles were synthesized using a coacervation technique. BSA was selected for its stabilizing properties and PEG for its ability to improve the anti-viral effects. The formulated NPs were readily dispersible in water and had a diameter smaller than 120 nm. Female Sprague-Dawley rats were administered PEG-BSA-NIC nanoparticles at a dosage of 2 mg/kg via injection. The control was a solution of NIC containing ethanol and ß-cyclodextrins. From the PK data, it is clear that the C_{max} could be reached in 15 minutes and that a systemic circulation of NIC could be retained up to 6 hours. On the other hand, NIC cleared very quickly with the control formulation. The C_{max} was improved to 904.74 ±117.52 from 723.67±354.83 ng/mL. T_{max} was the same for both

the new formulation and control, while $t_{1/2}$ improved 8.35-fold compared to control. However, it is interesting to note that the control had a higher *AUC*.

The same group (Rejinold et al) proposed a new hybrid formulation where they loaded NIC into exfoliated layered double hydroxide nanoparticles (X-LDH NPs).[67] The prepared X-LDH NPs were further functionalized with Eudragit S100 (ES100), as an enteric coating, (ES100-NIC-X-LDH NPs). This should improve the absorption by the gastrointestinal tract, by making it responsive at the intestinal pH of 6.8. Tween 60 was additionally applied as a coating onto ES100-NIC-X-LDH nanoparticles to improve their stability, mucoadhesive characteristics, and drug release profile. The final formulation, Tween 60-ES 100-NIC-X-LDH-NPs was intended for oral delivery addressing Covid-19. The final formulation, NPs, had particles with a mean diameter of 215.56 ±08.72 nm. Drug release studies were performed at pH 1.2 and 6.8, with the addition of 2% Tween 60 in both buffers. Under intestinal pH conditions, a notably higher release of NIC from ES100-NIC-X-LDH was observed, nearing complete release within 24 hours, contrasting with a limited release of approximately 30% at pH 1.2. When Tween 60 was present as a coating, the release of NIC from Tween 60-ES 100-NIC-X-LDH-NPs was much faster. Indeed, at pH 6.8 almost 100% of the drug was released in 1 hour, much faster and complete compared to pH 1.2. The authors noted that the heightened release of NIC at intestinal pH might be attributed to the enhanced stability and solubility achieved when NIC was combined with ES100 and Tween 60. Tween 60-ES 100-NIC-X-LDH-NPs was orally given to male Sprague-Dawley rats at a dosage of 50 mg/kg. NIC plasma concentration after oral administration of Tween 60-ES 100-NIC-X-LDH-NPs was such that the IC_{50} value could be maintained for at least 8 hours. Very high values of AUC_{last} were reached: 13924.76±4087.19 ng·h/mL. $t_{1/2}$ was 4.86±0.84H, C_{max} was 15328.82±6854.44 ng/mL and T_{max} was 0.60±0.22. The present formulation presented very high PK parameters compared to the commercially available Yomesan®, referred by the authors in another study.[7] Yomesan® presented a C_{max} of approximately 155 ng/mL, T_{max} was 4h and *AUC* of approximately 1100 ng·h /mL.

Choi et al designed NIC-loaded hydrotalcite composite nanohybrids, which were subsequently coated with Tween 60 or hydroxypropyl methylcellulose (HPMC).[62] They were designed for the oral administration towards Covid-19 infections. Hydrotalcite (HT) was selected for its biocompatibility and mucoadhesive properties. In this study, an attempt was made to increase the specific surface area of hydrotalcite (HT) by calcining it at around 300°C. This process aimed to remove interlayer and physisorbed water from the two-dimensional HT lattice, leading to the formation of dehydrated HT (DHT) with a significantly larger surface area compared to HT. Ultimately, NIC-DHT hybrids were produced with a drug loading of 43%. Subsequently, they were coated with either Tween 60 or HPMC, namely NIC-DHT/Tween 60 and NIC-DHT/HPMC. The average particle size of NIC-DHT was determined to be 292.7±28.3 nm. The PK studies were performed in male Sprague-Dawley rats. NIC-DHT/Tween 60 (50 mg/kg) and NIC-DHT/Tween 60 (or HPMC) (200 mg/kg) were orally administered. The control was the commercially available Yomesan® (50 mg/kg). Firstly, it is notable that the C_{max} for NIC-DHT/Tween 60 (at 50mg/kg) was 1350.37±613.98, whereas for Yomesan® it was 155.27 ±39.92, representing an 8.7-fold improvement. The AUC_{last} was 1823.83 ±305.26 for NIC-DHT/Tween 60 (at 50 mg/kg), and 1096.81 ±359.28 for Yomesan®. Additionally, T_{max} was also improved from 4 h for Yomesan® to 0.25 h for NIC-DHT/Tween 60 (50 mg/kg). When the dosage of NIC-DHT/Tween 60 was increased from 50 to 200 mg/kg, the plasma concentration of NIC above the IC_{50} level was sustained for up to 8 hours. However, by altering the coating of the formulation with HPMC, which has a better gastrointestinal retentive property than Tween 60, the NIC plasma concentration above the IC_{50} threshold was extended beyond 24 hours.

Lipid Nanoparticles, Liposomes and Nanoemulsions

Solid lipid nanoparticles (SLNs) are utilized as carrier systems for poorly water-soluble drugs and cosmetic active ingredients. They range in size from 10 to 1000 nm. Solid lipid nanoparticles (SLNs) are aqueous colloidal dispersions containing biodegradable solid lipids. They offer advantages such as improved physical stability, protection of labile drugs, controlled release, and enhanced tolerability. SLN formulations have been developed and thoroughly characterized for various administration routes, both in vitro and in vivo.[68] Liposomes are self-assembled phospholipid-based drug vesicles consisting of one or more concentric lipid bilayers enclosing discrete aqueous spaces, showing outstanding properties as drug carriers by protecting the encapsulated substances from physiological degradation, extending the half-life of the drug, controlling the

release of drug molecules and exhibiting excellent biocompatibility and safety. Many liposomal products are on the market with more under clinical development.[69]

Lipid emulsions consist of submicron colloidal particles typically ranging from 100 to 500 nm in size. Submicron lipid emulsions (SLEs) exhibit greater stability compared to alternative lipid carriers like liposomes and SLNs. They are considered safe for both oral and injectable applications.[70] Solid lipid nanoparticles offer the potential to enhance NIC absorption into the lymphatic system, thereby mitigating the first-pass effect by the liver. This prospect is commonly associated with lipid formulations, drawing upon the process by which dietary lipids are digested and subsequently absorbed in the intestine.[71] Incorporating and solubilizing NIC within a lipid matrix system has the potential to mitigate the impact of NIC crystal transformations, such as from anhydrous to monohydrate H_A, to H_B. However, this approach may entail lower drug loading compared to nanocrystals. For solid lipid nanoparticles, polymorphic changes in the solid lipid could be a critical factor in stabilizing the system.[72]

Zhang et al developed two different NIC-loaded submicron lipid emulsions (NIC-SLEs) for oral delivery.[70] Formulation modifiers such as oleic acid and poly (ethylene glycol) monooleate were utilized to create conventional submicron lipid emulsions (CSLEs) and PEGylated submicron lipid emulsions (PSLEs), respectively. NIC-SLEs were prepared through melt dispersion followed by high-pressure homogenization. The average particle size of NIC-CSLEs was 307.8±5.2 nm while that of NIC-PSLEs was 162.2 ±3.8 nm. Release studies were conducted at pH 6.8 using 2% Tween 80 as a solubilizer, both with and without pancreatic lipase (100 IU/mL) as the digestion of lipid carriers by gastrointestinal enzymes is physiologically unavoidable. The release of both NIC-SLEs in the lipase-free media was extremely slow, with the accumulative releases ranging from 0.49% to 1.30%. In the presence of pancreatic lipase in the release media, both NIC-SLEs showed a drug burst release within 5 minutes, with a release amount exceeding 7.5%. However, the release subsequently slowed down, and the cumulative release reached only 10.16% and 9.37% at 6 hours, respectively. It appeared that the final release was incomplete. To assess PEG's protection against lipolytic enzymes, a lipolysis of NIC-SLEs was performed. However, no significant differences were noted between formulations with or without PEG. This was attributed to the polymer's low molecular mass of just 1200. NIC exhibits moderate permeability across various intestinal segments, with the highest permeability observed in the duodenum, followed closely by the jejunum, ileum, and colon. Encapsulation of NIC into SLE significantly enhances its permeability. SLEs led to approximately 2-, 3-, 2-, and 4-fold increases in permeability in the duodenum, jejunum, ileum, and colon, respectively. The differences between NIC-CSLEs and NIC-PSLEs were only notable in the ileum and colon, where NIC-PSLEs exhibited higher values. The formulations were administered orally to Sprague-Dawley rats at a dose of 20 mg/kg. The relative bioavailability of NIC-CSLEs was 441.11% compared to the reference (NIC suspension), whereas NIC-PSLEs showed an even higher bioavailability of 463.55%. The AUC was approximately 2.5 μg·h/mL for both nanoemulsions compared to 0.5 for the suspension, resulting in a five-fold increase. Despite the difference in particle size, the bioavailability of the nanoformulations was very similar. NIC-PSLEs yielded a higher peak concentration (C_{max}) compared to NIC-CSLEs. The C_{max} values were 0.726 μg/mL for NIC-PSLEs and 0.432 μg/mL for NIC-CSLEs, respectively, compared to 0.195 μg/mL for the suspension. The authors noted an intriguing phenomenon wherein different carriers yielded the same enhancement of bioavailability. They suggested that the intrinsic cause of this bioequivalence could be attributed to the lipolysis of lipid carriers in the GI tract.

Rehman et al prepared solid lipid nanoparticles by micro-emulsion technique, using stearic acid (SA), polysorbate 80, and PEG.[73] The authors assessed four variables: the concentration of SA, polysorbate 80, PEG, and stirring time. Among the options evaluated, the formulation containing 66.6mg NIC, 1g SA, 1.6g Tween-80, and 0.4g PEG-400, with a stirring time of 15 minutes, was chosen for further studies. The final formulation gave an average particle size of 204.2±3.2 nm. The release study at pH 7.4 showed a sustained release (93.21%) of NIC in 12 hours. The selected formulation (NFM-3) and the marketed drug Mesan® were orally administered to rabbits at a dosage of 100 mg/kg. C_{max} values for the nanoparticles and the marketed drug were 3.97 and 1.84 μg/mL respectively. This represents a 2.15-fold increase. The $AUC_{0-\infty}$ for the nanoparticles was reported to be 16.74 μg h/mL compared to 1.51 for Mesan®, showing an 11.08-fold increase. Barbosa et al explained this result by suggesting that solid lipid nanoparticles might enhance the absorption of NIC into the lymphatic system, thereby reducing the first-pass effect by the liver. This hypothesis is grounded in the

process of lipid digestion from dietary sources and subsequent absorption in the intestine.[10] Finally, it is noteworthy to mention that P-XRD studies confirmed the amorphous nature of the NIC-loaded nanoparticles.

Pindiprolu et al engineered solid lipid nanoparticles for targeting breast cancer cells.[74] Stearylamine served as the solid lipid in the formulation of NIC-loaded solid lipid nanoparticles (NIC-SLNs). The emulsification-solvent evaporation technique was employed for the preparation of NIC-SLNs. NIC and stearylamine (solid lipid) were dissolved in methanol to form the lipid phase, while Tween 80 and Pluronic F-68 were dissolved in double-distilled water to form the aqueous phase. The two phases were then homogenized, sonicated, and freeze-dried to obtain NIC-SLNs. The formulation of NIC-SLNs was optimized using Box-Behnken experimental design. The particle size of NIC-SLNs was found to be 112–18 ±1.73 nm. The drug load and entrapment efficiency of NIC-SLN were determined to be 8.3±0.42% and 82.21±0.62%, respectively. Additionally, the particles were observed to be spherical in shape. The drug release profile was investigated at a physiological pH of 7.4 and acidic pH of 5.5 to simulate an acidic tumour microenvironment. At pH 5.5, an initial burst release was observed within the first hour, likely attributed to the drug attached to the surface. It's evident that at pH 5.5, the release was much more extensive compared to pH 7.4, with 90% of the drug released at pH 5.5, whereas only 25% of the drug was released at pH 7.4. The authors attributed this to the protonation of an amino group of stearylamine at lower pH values. Although no PK data were available, NIC-SLN notably inhibited the cell viability percentage and exhibited a lower CTC50 compared to NIC alone. The authors observed an accumulation of cells in the G0/G1 phase of the cell cycle in both NIC (69.50%) and NIC-SLN (77.06%) treated cells compared to control cells. Furthermore, NIC-SLN treatment (70%) significantly increased the percentage of apoptotic cells compared to naive NIC (50%).

Wang et al produced a lipid nanoparticle formulation of NIC addressed to inhibit SARS-CoV-2 replication in vitro.[75] The resulting formulation contained NIC: distearoyl phosphatidyl ethanolamine (DSPE)- PEG 2000 in a weight ratio of 1.19:1, which corresponds to 54.3% loading capacity. The particles had a diameter below 200 nm. Although no pharmacokinetic (PK) data were available, the authors investigated the in vitro efficacy against SARS-CoV-2 infection in Vero E6 and ACE2-expressing lung epithelial cells. The authors verified that the nano-NIC formulation demonstrated anti-viral efficacy against SARS-CoV-2 infection in human lung epithelial cell line A549 cells expressing human ACE2, with IC_{50} and IC_{90} values of 0.154 μM and 1.38 μM, respectively, while achieving a selectivity index of 137. Yu et al made slight modifications to the formulation (NIC-Lips) by incorporating cholesterol as an additional component. This adjustment aimed to create a smaller and more monodisperse formulation,[75] with the goal of addressing the reversal of pulmonary fibrosis.[76] TEM analysis demonstrated the round morphology and lipid bilayer structure of both the blank liposomes (Lips) and the NIC-Lips. The average particle size was 119.60 ±2.2 nm for the blank-Lips and 136.97 ±0.54 nm for the NIC-Lips. The fabricated NIC-Lips demonstrated stability when stored at 4°C for a minimum of 15 days. Additionally, as indicated by the authors, NIC-Lips displayed a slow cumulative release behavior. The encapsulation efficiency of NIC-Lips was 89.48 ±2.40%. The mass concentration of NIC in NIC-Lips was approximately 1 mg/mL. The formulation was further tested in vivo on rats. 1.0 mg/kg of NIC and NIC-Lips were administered via the tail vein. The peak blood concentration was achieved at 0.083 hours. The authors noted that this observation suggests the drug quickly enters systemic circulation following intravenous administration After intravenous administration to rats, the distribution of NIC-Lips in plasma and major organs, including the lungs, was examined. Despite NIC-Lips showing high expression in the plasma and liver, they are also distributed in lung tissue and can rapidly reach it shortly after administration. The authors observed that in other studies,[30] the tissue distribution of NIC was notably limited, with substantially higher concentrations found in the intestine, kidneys, and liver following intravenous administration of NIC (2 mg/kg). Moreover, the authors discovered that NIC-Lips could decrease the accumulation of immune cells (Gr1+CD11b+, MHC II+CD11c+, and M2 macrophages). These findings suggest that NIC-Lips may alleviate imbalances in the immune microenvironment and exert an anti-pulmonary fibrosis effect. Additionally, NIC-Lips can inhibit the activation of fibroblasts and the process of epithelial-mesenchymal transition (EMT) in lung epithelial cells.

Reddy et al developed a NIC stearate prodrug addressed against osteosarcoma.[77] NIC stearate is a prodrug of NIC (NICSPT), wherein a fatty acid stearate is covalently linked to NIC via an ester bond. In vivo this bond is expected to undergo hydrolysis, releasing free NIC. The nanoparticles were synthesized using a rapid solvent exchange method, whereby rapid precipitation spontaneously forms nanoparticles comprising a NIC stearate core coated with a lipid monolayer. The nanoparticle size was approximately 50 nm. The group's strategy was to convert the relatively water-insoluble NIC into its even less soluble stearate ester, with the expressed goal of creating injectable NICSPT

nanoparticles at doses of at least 50 mg/kg. 50 mg/kg NICSPT (corresponding to 27 mg/kg NIC equivalent) was injected intravenously in mice. The *AUC* for NIC stearate was 3560 µg·h/mL and for NIC 690 µg·h/mL. NIC stearate and NIC both had a similar half-life of 5 and 5.5 h respectively. The authors observed a significant decrease in metastatic burden and improved survival in mice with metastatic osteosarcoma at a low dose of just 0.59 mg/kg weekly. Furthermore, increasing the dose of 50 mg/kg showed no increase in toxicity. NICSPTs have demonstrated inhibition of osteosarcoma cell growth with IC_{50} values ranging from 0.2 to 2 µmol/L.

Shah et al loaded NIC into liposomes consisting of egg lecithin and cholesterol using a quality-by-design approach, resulting in vehicles of 153, 26 nm in size, with PDI of 0.201 and drug loading efficiency of 83.34%.[78] The liposomal NIC was further incorporated into thermo-responsive gel consisting of Pluronic F127 and Pluronic F68 at the 3:1 ratio. Incorporation into the liposomes facilitated enhanced melanoma cell uptake of NIC and consequent apoptosis. Cytotoxicity studies revealed a 1.756-fold enhancement in SK-MEL-28 cytotoxicity by NIC-loaded liposomes compared to free drug. Qualitative and quantitative cell internalization indicated greater drug uptake within the melanoma cells illustrating the high efficacy of liposomes as carrier systems. Nuclear staining showed blebbing and membrane shrinkage. Elevated ROS (reactive oxygen species) levels and apoptosis shown by DCFDA (dichlorodihydrofluorescein diacetate) and acridine orange-ethidium bromide staining revealed greater melanoma cell death caused by liposomal NIC compared to free drug. Sustained zero order release up to 48 h with liposomes and a 23.58-fold increase in viscosity caused by the sol-to-gel transition at 33°C was observed for liposomal thermogel. Ex vivo gel permeation studies revealed that C-6 loaded liposomes incorporated within the thermogel successfully formed a depot over the upper skin layer for 6 h to prevent transdermal delivery and systemic adverse effects. Thus, it appears that NIC-loaded liposomal thermogel system could be an efficacious therapeutic alternative for the management of melanoma, ensuring localized drug delivery to the upper skin layers.

Elkholi et al recently developed chitosan-coated nanostructured lipid carriers (NLCs) for the targeted delivery of NIC in breast cancer cells.[79] The preparation of NLCs involved utilizing the micro-emulsification technique, incorporating Precirol ATO 5 (low melting point) and Compritol 888 ATO (high melting point) as solid lipids, along with oleic acid and Tween 80 as liquid components. Additionally, diacetyl phosphate was used as a charging agent to facilitate the coating process. Three formulations of uncoated nanoparticles, labelled as F1, F2, and F3, were prepared with escalating amounts of Tween 80 (0.3 g, 0.4 g, and 0.5 g, respectively). Additionally, formulations F4 and F5 were coated with chitosan, with Tween 80 amounts of 0.3 g and 0.4 g, respectively. The average particle sizes of the uncoated NLCs were 226.4 nm, 189.6 nm, and 334.5 nm for formulations F1, F2, and F3, respectively. The authors attributed the significant rise in particle size following the incorporation of a high concentration of Tween 80 (F3) to a potential increase in the viscosity of the interfacial film, which may lead to an enlargement of microemulsion droplets. Chitosan coating led to an increase in particle size compared to the corresponding uncoated particles. Formulations F4 and F5 exhibited particle sizes of 268 nm and 259.5 nm, respectively. Findings from Fourier transform infrared spectroscopy (FTIR) indicated the presence of hydrogen bonding between NIC and NLCs components. Interestingly, chitosan coating did not induce any additional alterations in the spectral pattern of NIC, as anticipated, given that the drug is situated within the lipid core of NLCs. Differential scanning calorimetry (DSC) findings indicate the amorphization of the drug or its solubility within the solid and/or liquid lipid components of NLCs. The entrapment efficiencies were 99.1%, 99.2%, and 98.8% for the uncoated formulations (F1, F2, F3, respectively), and 99.6% and 99.7% for the coated formulations F4 and F5, respectively. The authors remarked that the achieved high entrapment efficiency is satisfactory, given the lipophilic properties of NIC, which typically reside within the lipid matrix. This high efficiency reflects excellent drug retention and the absence of expulsion during lipid chain crystallization. The presence of liquid lipid, considered advantageous for NLCs over solid lipid nanoparticles, contributes to this enhanced retention. Release studies were conducted in phosphate buffer pH 7.4 with 2% Tween 80, lasting 10 hours. All formulations exhibited notably slow liberation of NIC, with total amounts released ranging from 3% to 5%. The authors attributed this slow release to the lipophilic nature and poor dissolution of NIC. Interestingly, there was no significant difference observed between the release profiles of coated and uncoated NLCs. This is attributed to the preferential localization ofNIC within the lipid matrix of NLCs. Consequently, the drug release is governed by the relative affinity of NIC to the lipid matrix compared to the external aqueous environment. This phenomenon elucidates the lack of a significant effect of chitosan coating on NIC release. Except for formulation F3, the

formulations were evaluated in vivo and orally administered to mice bearing the Solid Ehrlich carcinoma model. On day 26, tumor volume decreased by 79%, 76%, 73%, and 75% for formulations F1, F2, F4, and F5, respectively. These findings demonstrate a significant reduction in tumor volume compared to the control group receiving an aqueous suspension and the untreated group. Moreover, the NLCs formulations exhibited comparable efficacy. The tumor weight was significantly reduced compared to both the simple suspension and untreated groups. Analysis of the histopathological sections revealed that the extent of necrosis indicated the superiority of the particulate system over the drug suspension, with the coated system exhibiting greater efficacy. The reduction in mitotic figures was notably significant compared to the untreated control, underscoring the superiority of NLCs over the drug suspension. Formulations containing higher proportions of Tween 80 exhibited increased effectiveness. Moreover, the tumor giant cell score was significantly diminished across all tested formulations, with consistent rankings observed. The authors proposed that the enhanced effectiveness of chitosan-coated NLCs compared to the uncoated ones seen in the histopathological changes in tumor cells could be attributed to the mucoadhesive properties of chitosan-lipid nanoparticles and nanoemulsions.

Cyclodextrins and Dendrimers

Biomedical and pharmaceutical cyclodextrins (CDs) are cyclic oligosaccharides composed of six to eight dextrose units (α-, β-, and γ-CDs), linked through α −1,4 glycosidic bonds.[80] CDs find applications in the pharmaceutical industry for enhancing drug solubility, improving dissolution rate, increasing bioavailability, masking undesirable organoleptic properties, and more.[81]

Lodagekar et al investigated the role of hydroxypropyl-β-cyclodextrin (HPβCD) inclusion complex for improving the performances of NIC after oral administration as an anticancer therapy.[82] The complex was prepared using the freeze-drying method, with a slight modification involving the addition of 10 mM ammonia during the equilibrium period to solubilize NIC. This step resulted in an enhanced drug loading of 63% and a less bulky product. The absence of ammonia residue in the final product was confirmed. Phase solubility studies showed that plain NIC had a solubility of 8 µg/mL. The solubility of NIC significantly improved to 75 µg/mL with the presence of HP-β-CD, at 0.25 M concentration of CD. In vitro dissolution testing of NIC, physical mixtures, and NIC/HPβCD inclusion complexes with molar ratios of 1:1 and 1:2 was conducted in a pH 7.4 buffer containing 2% Tween by using a USP type II apparatus. The HPβCD complexes (1:1 and 1:2) exhibited 90% drug release within 30 minutes, whereas pure NIC showed only 36% release. This signifies a threefold increase in dissolution within the initial 30 minutes. Complete drug release was achieved in 90 minutes for the 1:1 complex and in 45 minutes for the 1:2 complex, compared to pure drug which showed only 75% release after 5 hours. BALB/c mice were orally given NIC in the form of suspension or NIC HPβCD complex (1:1) at a dose equivalent to 50mg/kg. The formulation resulted in a notable 1.33-fold increase in the C_{max} of NIC compared to the plain drug. The authors credited this enhancement to the increased solubility and accelerated release of NIC from the complex formulations. The rapid drug release led to a significant reduction in T_{max} from the formulation (0.28 hours) compared to plain NIC in suspension form (0.58 hours). Interestingly, no significant difference was observed in the *AUC* of NIC between the complex formulation and the plain drug, suggesting that the extent of drug absorption was similar from both the formulation and the drug in suspension form. The authors noted that since there was a decrease in IC_{50} values for the formulation compared to plain NIC, the formulation successfully delivered NIC.

Xie et al endeavoured to enhance the solubility and dissolution characteristics of NIC for the treatment of skin cancer by employing octenylsuccinate hydroxypropyl phytoglycogen (OHPP).[83] OHPP, a derivative of phytoglycogen (PG), a naturally occurring dendrimer-like polymer sourced from various plants. It was selected for its capacity to encapsulate and disperse insoluble phytochemicals, thereby augmenting their solubility and permeability. OHPP synthesis involved the grafting of hydroxypropyl and octenylsuccinate groups onto PG particulates. The preparation of NIC-solubilizer solid dispersion (SD) entailed a method wherein NIC and the carrier (OHPP, hydroxypropylmethylcellulose acetate succinate (HPMCAS), or Soluplus®) were dissolved in ethanol and subjected to spray-drying to obtain the solid form. Additionally, a physical mixture (PM) of NIC and OHPP (referred to as NIC/OHPP PM) was produced by blending NIC and OHPP solids at a weight ratio of 1:2. The phase solubility of NIC in phosphate buffer (pH 6.8, 58mM) increased linearly with rising concentrations of OHPP (0 to 100 mg/mL). At the highest OHPP concentration (100 mg/mL), NIC solubility reached 113.3 µg/mL, a significant 117-fold increase compared to solubility in phosphate buffer alone (1.14 µg/mL).

X-ray crystallography results for NIC-OHPP PM exhibited a diffraction pattern resembling that of pure NIC, indicating its crystalline nature. In contrast, NIC-OHPP SD showed a predominantly amorphous state for NIC. Additionally, FTIR analysis confirmed the absence of interactions between NIC and OHPP in their physical mixture. When comparing the solubility of solid dispersions at a total NIC concentration of 2.5 mg/mL in phosphate buffer of pH 6.8, the solubility of NIC was measured as 0.34 µg/mL, 34.2 µg/mL, 5.3 µg/mL, and 1723.6 µg/mL for NIC alone, NIC-HPMCAS SD, NIC-Soluplus SD, and NIC-OHPP SD, respectively. These findings underscore the superior solubilizing capability of OHPP for NIC. In phosphate buffer pH 6.8, the dissolution profile of NIC unfolded as follows: NIC alone showed a cumulative dissolution of 0.51% within 180 minutes. In contrast, for NIC-OHPP SD, 50.7% of NIC dissolved within just 15 minutes, with the dissolution percentage reaching 61% by the end of 180 minutes. Remarkably, at the 180-minute mark, the amount of dissolved NIC from NIC-OHPP SD was 120 times greater than that of NIC alone. The authors attributed the successful outcome of NIC-OHPP SD to potential interactions between OHPP and NIC, likely facilitated by hydrophobic interactions and hydrogen bonding. Such interactions have the potential to stabilize NIC in the amorphous state, contributing to its enhanced solubility and dissolution characteristics. The IC_{50} values for NIC-OHPP SD in comparison to DMSO-assisted NIC solutions indicated heightened cytotoxicity of NIC-OHPP SD against HeLa, PC-3, and A549 cells. Additionally, during simulated skin testing, the cumulative permeation of NIC with NIC-OHPP SD was 5.3 times greater than that of NIC alone.

Yang et al investigated the impact of 4-sulphonato-calix(n)arenes, cyclodextrins, and their combination on the aqueous solubility of NIC.[84] The authors observed that the solubility of NIC increased when combined with 4-sulphonato-calix(n)arenes. Additionally, among cyclodextrins, HP-β-CD exhibited the most significant effect in enhancing NIC solubility. To further augment NIC solubility, the authors combined these two complexes, forming 4-sulphonato-calix (6) arene:CD complexes. This combination led to an additive increase in solubility, surpassing the solubility enhancements achieved by the individual excipients. Particularly successful combinations were noted when 4-sulphonato-calix (6) arene and HP-β-CD were paired, attributed to strong interactions between NIC and calixarenes and cyclodextrins, primarily involving hydrogen bonding and hydrophobic interactions.

Polymeric Nanoparticles

Polymeric nanoparticles (PNPs) are synthesized using biocompatible and biodegradable polymers, ranging in size from 10 to 1000 nm. Within these nanoparticles, drugs are either dissolved, entrapped, encapsulated, or attached to a nanoparticle matrix. The method of preparation determines whether nanoparticles, nanospheres, or nanocapsules are produced. Polymer-based nanoparticles serve as efficient carriers for transporting drugs, proteins, and DNA to specific cells and organs. Their nano-scale dimensions facilitate enhanced permeation through cell membranes and ensure stability within the bloodstream.[85]

Gan et al developed a codelivery nanoparticles composed of a biodegradable poly (E-caprolactone, E-CL)-poly (ethylene glycol)-poly(E-CL) (PCEC) triblock copolymer system, which was loaded with NIC, for the intravenous administration to treat pulmonary fibrosis.[86] The NIC-loaded nanoparticles (NIC-NPs) were prepared by the emulsification solvent evaporation method. The average particle size of NIC-NP was determined to be approximately 172 nm. Drug loading and encapsulation efficiency were reported to be approximately 14% and 93% respectively. Release studies were performed in PBS buffer at a pH of 7.4 containing 0.5% v/v Tween 80. NIC-NPs had a slower cumulative release and around 70% of the drug was released after 120 h. NIC alone showed a faster release with approximately 90% of the drug being released after 120h. The authors mentioned that NIC-NPs enhanced the water solubility of NIC, facilitating better dispersion in aqueous solutions. However, this improvement was not quantified and relied solely on visual observation. The new formulation proved to be equally successful, as a lower dose of NIC-NPs (2.5 mg/kg) demonstrated the same efficacy in reversing established pulmonary fibrosis as the free NIC (5 mg/kg) after peritoneal injection in mice.

Naqvi et al developed NIC-loaded chitosan nanoparticles for the treatment of cancer.[3] Chitosan cargo was cross-linked with glutaraldehyde, the nanoparticles were prepared via the desolvation method using sodium sulfate as a precipitating agent. The addition of polysorbate 80 was necessary to stabilize the nanoparticle solution. NIC-Chi NPs had a diameter of 100–120 nm with a spherical shape. NIC-Chi NPs appeared as a clear, dispersed formulation while free NIC had macroscopic undissolved flakes of the drug in aqueous media. Crystal studies indicated that the drug-loaded

chitosan nanoparticles exhibited an amorphous structure, in contrast to the crystalline nature of NIC alone. The authors suggested that this could be attributed to cross-linking among the reactive functional groups (amine groups) and drug molecules, in addition to hydrogen bonding and electrostatic interactions between them. The release studies were conducted under two pH conditions: physiological pH 7.4 and endosomal pH 5.5. NIC showed greater release under acidic conditions compared to physiological conditions. Specifically, only 15% of the drug was released over 7 days at pH 7.4, while almost 90% of the loaded drug was released at pH 5.5. The authors attributed this trend to the protonation of an amino group of chitosan at lower pH values. They further explained that minimal drug release occurs in the bloodstream, with the majority of release happening when NIC-Chi NPs reach the mildly acidic tumor microenvironment. The therapeutic effectiveness of NIC-Chi NPs was assessed against two cancer cell lines: MCF-7 (breast cancer) and A549 (lung cancer). The IC_{50} values obtained were reported as 8.75 μM and 7.7 μM, respectively.

Bhushan et al developed a NIC-encapsulated bovine serum albumin nanoparticle (BSA-NIC NPs) for cancer therapy.[87] BSA-NIC NPs were synthesized using the desolvation method. Ethanol was used as the desolvating agent and glutaraldehyde as the crosslinking agent. The particles had an average diameter of 199.9 nm. They were spherical in shape with uniform size distribution. In contrast, pristine NIC showed a micrometer size rod shape flake. X-ray diffraction studies revealed an amorphous nature of BSA-NIC NPs compared to NIC alone. The authors noted that the cross-linking mechanism among the reactive functional groups of protein and drug molecules, coupled with significant hydrogen bonding interactions between them, might contribute to the amorphous nature of the albumin particles loaded with the drug the encapsulation efficiency was 92.36% with NIC: BSA ratio of 12:25. Drug release studies were carried out at pH 7.4 for 96 hours. They revealed a biphasic drug release pattern: an initial burst release of 37.15% occurred within the first 10 hours, succeeded by sustained drug release. The burst release was attributed to surface-bound drug molecules, while the controlled release was credited to encapsulated drug molecules. Within the subsequent 24 hours, cumulative release steadily reached 74.81%. After 4 days, the cumulative release amounted to approximately 73%. The authors attributed the enhanced stability of the BSA-NIC-NPs in the physiological buffer to the cross-linking mechanism of the protein nanoparticles using glutaraldehyde. Stability studies in aqueous and 0.9% saline solution showed no obvious size change in 96 h. The IC_{50} values for BSA-NIC-NPs were determined to be 5 μM for A549 cells and 2.6 μM for MCF-7 cells. Bare NIC exhibited non-toxic effects, likely due to its insolubility. BSA -NIC NPs were shown to successfully induce apoptosis of treated cancer cells.

Misra et al synthesized innovative nanoparticles encapsulating NIC, a STAT3 blocker, and amonafide, a topoisomerase-II inhibitor, for targeted therapy against triple-negative breast cancer.[88] They described the synthesis of "hyperstar polymers (HSP)" through sequential atom transfer polymerization. The concept aimed at fabricating HSP as nanocarriers, wherein hyperbranched macro-initiators were polymerized to generate a core-shell structure to encapsulate the two compounds. The shell, designed for water dispersion, consisted of protonable tertiary amine groups. Meanwhile, the core comprised acid-degradable acetal groups, facilitating drug release under acidic conditions. In the results, the combination exhibited a synergistic effect against TNBC cells. The IC_{50} was approximately 5 μM for BT-549 and approximately 1 μM for MDA-MB231, compared to MCF-7 and SKBR-3 cells where the IC_{50} was approximately 30 and 20 μM, respectively.

Nanofibers

Polymer nanofibers exhibit promising characteristics as drug delivery systems due to easy preparation by electrospinning technology, adjustable features of wettability and elasticity, tailored surface and interface properties, and high surface-to-volume ratio for mass transfer enabling programmable drug release. Their similarity with natural fibrillary extra-cellular matrix facilitates cell adhesion making them a suitable platform for tissue regeneration. The most common biomedical application of polymeric nanofibers involves the local delivery of poorly soluble medicines, like antibiotics and antitumoral drugs, as well as nanofiber use in the development of wound dressings.[89] Kumar and Gopinath developed a nanofiber-based scaffold for the delivery of drug-polymer complex. Hydrophilic branched polyethyleneimine-NIC (bPEI-NIC) complex was pre-synthesized and stabilized by crosslinking with glutaraldehyde and was then incorporated into composite bPEI/PEO (poly(ethylene oxide) 900 kDa) nanofibers by electrospinning.[90] The obtained nanofibers with a uniform diameter of 430±47 nm were then further crosslinked with glutaraldehyde to modify bPEI-NIC release. The

degree of crosslinking and the NIC loading level enabled modulation of the in vitro release of NIC by changing the drug release mechanism from Fickian diffusion (10 s cross-linked fibers) to non-Fickian anomalous transport (30 s cross-linked fibers). The antitumor efficacy of the developed nanofibers was then tested on A549 (non-small cell lung cancer cells) and U-87 MG (glioblastoma cells) showing a decrease in cell viability when treated with nanofibers containing increased drug dose.[90] In the following studies, authors developed composite PEO-bPEI electro-spun nanofibers that besides the drug also contained silver nanoparticles[91] or folic acid functionalized octagonal magnetite nanoparticles,[92] all enabling to further enhance the anticancer effect of such nanofibers. Moreover, PEO served as a template for the in-situ synthesis of silver nanoparticles, while in the case of folate-decorated magnetite nanoparticles, their synthesis and functionalization needed to be performed before the electrospinning procedure. Although such a combined approach enabled potentiated NIC anticancer effect in vitro as well as targeted delivery in the case of nanofibers containing folic acid functionalized octagonal magnetite nanoparticles, the overall toxicity of such nanofibers still needs to be assessed.

Coban et al developed Eudragit L100 electrospun nanofibers with NIC, loading the drug alone, its physical mixture with HPβCD, or as a NIC/HPβCD inclusion complex.[93] As both the polymer and NIC are insoluble at low pH, it was presumed that the obtained nanofibers would not release the drug at gastric pH, but in vitro experiment showed substantial NIC release in an acidic medium of up to 53% of the loaded drug dose in case of the nanofibers loaded with the pure drug. The addition of cyclodextrin to the formulation reduced the unwanted NIC release at the acidic stage to only 15 and 8%, respectively, depending on whether the drug was incorporated as a physical mixture or an inclusion complex. When the pH of the release medium was raised to pH 7, mimicking the colon environment, the drug release was complete within 120 minutes due to the complete disintegration of nanofibers due to the pH-mediated dissolution of Eudragit L 100. Based on the observed in vitro release profile nanofibers containing HPβCD may be a suitable carrier for colon-targeted delivery of NIC in colorectal cancer treatment.

Dry Powders for Inhalation

The pulmonary route has been a longstanding method for drug administration, catering to both local and systemic treatment needs. It offers numerous advantages, which can be classified into physiological benefits, such as a large surface area, thin epithelial membrane, high vascularity, and limited enzymatic activity, as well as patient convenience factors, such as non-invasiveness and the ability for self-administration compared to oral and systemic routes of drug delivery.[94] For more than six decades, dry powder inhalers (DPIs) have been reliably treating patients worldwide. Over this time, the core principles of DPI formulation have remained unchanged: drugs are formulated into powders with particles sized for lung deposition.[95]

Ray et al developed an inhalable NIC-NCT formulation that has been previously described in the section "co-crystals",[45] while an inhalable dry powder formulation of NIC that was developed by Costabile et.al[53] that was already presented in the section "nanocrystals". Here we are reporting other types of formulations that are intended for the pulmonary delivery of NIC.

Jara et al developed a dry powder formulation of NIC using thin-film freezing (TFF) for administration via inhalation for the treatment of Covid-19.[5] TFF is a particle engineering technology primarily employed to craft inhalable powders intended for use with dry powder inhalers (DPIs). These, exhibit exceptional aerosol performance and are generated by rapid supercooling of drug-carrier solutions. The frozen material is subsequently subjected to lyophilization to eliminate the solvents utilized in the process. Mannitol and L-leucine were used in this study to enhance the aerosolization properties. The aerosol performance of the NIC inhalation powder was evaluated using the Next Generation Impactor (NGI). The powder exhibited a fine particle fraction (FPF) of 86.0% ± 2.7%. This is a notably higher value compared to other NIC inhalers manufactured using technologies such as high-pressure homogenization and spray drying.[45,53] The attained mass median aerodynamic diameter (MMAD) was approximately 1 μm, enabling it to reach the final stage of the cascade impactor. The authors' objective was to target the deep lung region to cover the majority of surfaces potentially infected by SARS-CoV-2, and this outcome indicates that it is achievable with this formulation. A three-day multi-dose tolerability and exposure study was conducted in female Sprague-Dawley rats. The administered dose was 200 μg per rat daily for three consecutive days. While there were indications of mild to moderate inflammation, the overall assessment deemed the formulation to be safe. Syrian hamsters were given doses of 8.7 or 17.4 mg/kg of NIC inhalation powder

each (equivalent to 145 and 290 µg/kg of pure NIC, respectively). The powder was administered intratracheally using the Penn-Century dry powder insufflator TM DP-4. The device was activated three times to deliver 200 µL of air per actuation. From the in vivo plasma pharmacokinetic parameters, it's evident that NIC was rapidly absorbed and cleared, leading to steady, low levels. This rapid absorption and clearance are viewed as advantageous in terms of safety and minimizing systemic side effects. A non-compartmental analysis of the plasma data was performed. The *AUC/dose* of both administered doses was similar (8.6 and 8.4) and clearance was also in the same range (116 and 119 mL/h). The plasma C_{max} values were 159 ng/mL and 590.3 ng/mL for the lower and higher administered doses, respectively. The reported AUC_{last} values were 83.3 ng·h/mL and 237.1 ng·h/mL for the lower and higher doses, respectively. The in vivo pharmacokinetic parameters in the lungs were as follows: the T_{max} remained consistent for both doses, reported at 0.25 hours. The C_{max} values were 20.5 and 37.2 µg/g of wet tissue, while the AUC_{last} was reported as 72.1 and 37.5 µg·h/g of wet tissue for the lower and higher doses, respectively.

Interestingly, the authors observed that after 2 hours, the lower administered dose exhibited a higher $AUC_{0\text{-}24}$ without reaching a higher C_{max}. They hypothesized that administering a higher dose of powder might have altered the aerosolization properties of the dry powder insufflator used to administer the powder to the hamsters. Doubling the dose of NIC via lung insufflation nearly doubled its C_{max}, but also more than doubled the plasma $AUC_{0\text{-}24h}$. This suggests increased clearance of the drug from the plasma rather than retention in lung tissue. This supports the authors' argument that higher doses may deposit the powder in larger airways, impacting pharmacokinetics by increasing clearance. This approach can lead to a reduction in first-pass metabolism. The authors emphasized that for therapeutic efficacy against SARS-CoV-2, the NIC inhalation powder should reach a concentration exceeding 0.154 µg/g. Their formulation surpassed this concentration in lung tissue by approximately 15 times with the lower dose and 2-fold with the higher dose over the 24-hour period. Moreover, the NIC inhalation powder maintained concentrations above the IC_{50} and IC_{90} values for at least 24 hours.

Brunaugh et al developed composite particles containing NIC and human lysozyme (hLYS) for the delivery ofNICin the upper and lower airways via dry powder inhaler, nebulizer and nasal spray, targeting coronavirus infection.[54] The dry powder was acquired using the spray drying technique, a method extensively studied for generating particles ideal for pulmonary delivery. Histidine (as a buffering agent), sucrose (as a lyoprotectant agent), and polysorbate 80 (as a surface-active agent) were employed to create a stable and dispersible formulation. The geometric median diameter of the optimized formulation was less than 5 µm. A commercially available dry powder inhaler (DPI), the TwinCaps ® (Hovione), was chosen for the inhalation delivery of NIC-hLYS. The NIC-hLYS was delivered with a fine particle dose of 136.0 ± 4.3 µg of NIC (ie, recovered drug mass with an aerodynamic diameter of less than 5 µm) achieved per 60 mg of total powder actuation (with 0.7% NIC content). For patients requiring mechanical ventilation, NIC-hLYS particles were evaluated utilizing an AerogenSolo® vibrating mesh nebulizer, which can be integrated into a ventilator circuit. The NIC-hLYS powder, reconstituted in 0.45% sodium chloride to a concentration of 25 mg/mL (equivalent to 175 µg/mL NIC), resulted in the delivery of a fine particle dose of 62.3 ±3.7 µg of NIC after a 2-minute runtime. Additionally, a range of concentrations (10 to 100 mg/mL) could be effectively emitted using the AerogenSolo® device. This flexibility is advantageous for pediatric patients and those with hepatic and renal insufficiency as the dose can be adjusted accordingly. The authors also suggested delivering the formulation via nasal spray. This is because the epithelial cells of the upper respiratory tract, particularly the nasal passage, demonstrate significantly higher expression of ACE2 receptors compared to those of the lower respiratory tract. This higher expression suggests that these tissues might be more susceptible to infection with SARS-CoV-2. The potential for administering the NIC-hLYS formulation via nasal spray was evaluated through a spray pattern and plume geometry analysis. NIC-hLYS powders were reconstituted in 0.45% sodium chloride at concentrations ranging from 10 to 50 mg/mL and dispensed using a VP7 Aptar® nasal spray device. Uniform spray patterns and appropriate plume angles for nasal administration were achieved across all tested concentrations. A slightly hypotonic reconstitution medium was chosen and applied in the in vivo studies to enhance absorption and potentially facilitate nose-to-brain penetration of NIC-hLYS. The dissolution rate of NIC-hLYS particles, which had an aerodynamic diameter of approximately 2 µm, was contrasted with that of NIC particles devoid of hLYS in a simulated lung fluid medium. The presence of hLYS in the formulation led to a marginally accelerated dissolution rate, with 82.1% of the deposited NIC dose dissolved within 6 hours. Although the formulation underwent in vivo testing, no

pharmacokinetic (PK) data was provided. The in vivo efficacy of NIC-hLYS particles was evaluated in lethal infection models for both MERS-CoV and SARS-CoV-2. HDDP-4 transgenic mice were employed to examine the effect of MERS-CoV, while HACE-2 transgenic mice were utilized to study the effect on SARS-CoV-2. The formulation was administered intranasally at various dosages (up to 240 micrograms/kg). In both MERS-CoV and SARS-CoV-2 infected models, lung tissue from mice treated with NIC-hLYS exhibited lower levels of interstitial pneumonia compared to infected mice that did not receive treatment. The combination of hLYS and micronized NIC in a co-formulation resulted in a fourfold increase in potency against coronaviruses and a twofold increase in potency against *Methicillin-resistant Staphylococcus aureus* (MRSA) compared to NIC particles alone.

3D Printing Technology

3D printing technology gained growing interest in the pharmaceutical field where it has been used to fabricate different drug delivery systems and dosage forms, often referred to in the literature as printlets (ie 3D printed tablets). This technology is based on layer-by-layer fabrication of objects that are digitally designed and is mainly used to fabricate oral dosage forms, providing benefits such as on-demand manufacturing, dosage flexibility, and the possibility to strategically incorporate different drugs within predetermined sections of the layers. The product manufacture may be obtained in fewer processing steps, resulting in an improved quality of the 3D printed dosage forms.[96]

Pistone et al applied direct powder extrusion (DPE) 3D printing technology to produce printlets providing sustained release of NIC. This innovative, one-step technology enabled the extrusion of the powder mixture containing NIC (10%, w/w), Hypromellose as a carrier polymer, HP-β-CD as solubilizing and complexing agent and PEG 6000 as a plasticizer using 3DForMe® 3D printer operating at 180 °C.[97] The thermal and mechanical stress caused by the printing process did not interfere with the NIC chemical stability. Solid state characterization of the printlets revealed complete amorphization of the NIC probably favored by the formation of NIC/HP-β-CD/Hypromellose ternary complex, which significantly enhanced the drug solubility. Although the extruded filaments showed some variation in the NIC content (6.34–13.57%, w/w), due to the demixing of the raw materials during the printing process, this was compensated in the printlets that were characterized by acceptable weight variation and drug content, as well as exceptional hardness and low friability. In the developed printlets, the drug remained amorphous and chemically stable for up to 3 months. HP-β-CD containing formulations achieved complete NIC release within 24 h, while in the formulations where HP-β-CD was not contained, the amount of the released drug in the same period ranged from 65% to 70%, requiring 48 h for the complete drug release.

Real et al used melting-solidification 3D printing technology to develop floating 3D printlets loaded with NIC, aimed at treating *Helicobacter pylori* infection.[98] To improve the drug solubility, NIC was first subjected to wet milling using Poloxamer 188 as a stabilizer at 1:1 drug-to-surfactant ratio, resulting in nanocrystals of 188.5 nm in size and a PDI of 0.186. Biocompatibility studies using human gastric adenocarcinoma cell lines (ATTC® CRL-1793TM) and immortalized human gastric epithelium cells demonstrated the reduced toxicity of NIC nanocrystals compared to the unmilled drug, which was attributed to the coating of the drug particles by Poloxamer 188 during nanoization. Unfortunately, the authors did not investigate how the nanoization of NIC affects its antimicrobial activity against *H. pylori*. The pure drug and freeze-dried NIC nanocrystals were then incorporated into Gelucire 50/13-based ink by fusion, allowing incorporation of up to 25% (w/w) of the drug dose in printable ink without compromising NIC nanocrystal structure. The 3D printing was performed at 47 °C, allowing the ink that was initially solid inside the syringe to be transformed into a semisolid material with a suitable viscosity to be extruded through a needle, forming a filament without collapsing on a printing bed. After its solidification at room temperature, the process is repeated layer by layer until the desired 3D shape is achieved. The printlets obtained with the ink containing drug nanoparticles demonstrated controlled release up to 12 h, while the release of the NIC from the printlets formulated with the pure drug was incomplete, reaching less than 20% of the incorporated drug dose in 12 h. Finally, gastroretention for developed printlets up to 180 minutes was demonstrated in dogs. The proposed technology combines the advantages of increased solubility and dissolution produced by the nanoization of NIC with facilitated nanocrystal powder handling, doze customization and gastroretention functionality. However, the exact therapeutic potential of such developed printlets loaded with NIC still needs to be further investigated. Finally, a regulatory framework for 3D-printed medicines and adequate quality assurance protocols still need to be defined to address all the possible risks and provide safe and efficient medication.[96]

Discussion

NIC was originally developed and marketed by Bayer in the late 1950s as a molluscicide, while therapeutic efficiency against tapeworms in humans was discovered later, leading to its registration as Yomesan® chewable tablets for humans in 1962. However, recent studies revealed the pleiotropic pharmacological activity of NIC, owing to its ability to regulate multiple signaling pathways and biological processes, leading to anticancer activity, metabolic regulatory activity, immunotherapeutic activity, antiviral and antibacterial activity.[99] Consequently, significant efforts have been made to reposition NIC by extending its therapeutic indications, with a particular focus on its anticancer[10,100] and antiviral activity.[29] Although "drug repositioning" is a strategy that enables the discovery of new biological effects of known drugs, through lower cost and time constraints, it is not without risks. In the case of NIC, the main risks are in the particular physiochemical properties of the drug and related low oral bioavailability. When used to treat tapeworm infections, NIC is administered orally in doses of up to 2 g, presenting efficacy and safety due to its local action in the gastrointestinal tract, as its intestinal absorption is limited and the adsorbed portion is rapidly eliminated by the kidney.[99] However, to treat cancer or acting antimicrobial, systemic delivery of NIC is required. Schweitzer et al tested NIC in combination with enzalutamide for castration-resistant prostate cancer (CRPC).[27] Even when NIC was administered at the maximal tolerated dose of 500 mg three times a day, the C_{max} among the patients ranged from 35.7 to 182 ng/mL, which is significantly below IC_{50} value for CRPC of 330 ng/mL that has been determined as effective in preclinical studies of the anticancer effect. This example clearly underlines the need to develop new and advanced NIC formulations, able to increase the solubility and consequently the oral bioavailability of the drug, or to provide localized drug release in a controlled manner providing the required drug concentration at the action site.

In this review, we have summarized different formulation approaches used to mitigate the low oral bioavailability of NIC. Different approaches were used, ranging from NIC chemical modification and prodrug synthesis, formulation of solid dispersion and co-crystals, as well as the development of novel nanosized drug delivery systems like nanocrystals, micelles, polymeric and lipid nanoparticles as well as cyclodextrin and dendrimers, 3D printed tablets and nanofibers.

Figure 3 presents the distribution of the types of formulations that were developed and analyzed in our review. There is a minor prevalence of derivatives, with no formulation standing out for having a significant abundance. Regarding the administration route, out of the 56 formulations tested, 24 either did not specify the administration pathway or were limited to initial studies. Figure 4 depicts the administration routes of the remaining 33 formulations. There is a noticeable trend in formulating NIC for the oral route. This is unsurprising, given that it represents the most compliant route for patients.

In general, each of the systems developed presented some benefit to NIC delivery, however, it is difficult to individuate the most effective approach. Indeed, numerous variables exist among the studies, hindering direct comparison. These include variations in animal models, administered dosages, solvents, pH levels during experimentation, the utilization of solubilizers like Tween 80 in certain studies but not in others, as well as a multitude of diverse therapy targets. NIC nanonization and inclusion complex formation appear particularly effective as demonstrated by Ye et al[25]

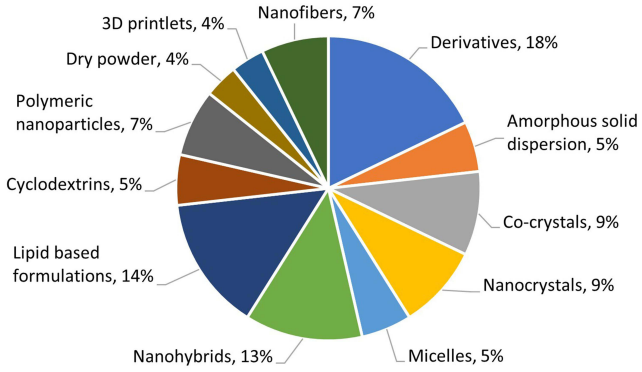

Figure 3 Distribution of NIC formulations reported in this review.

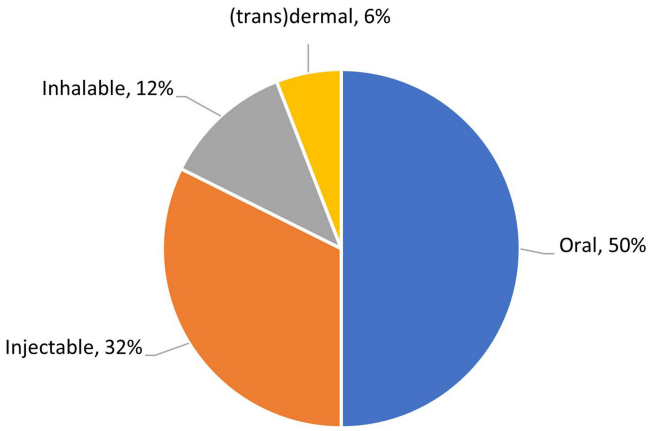

Figure 4 NIC administration pathways of the formulations reported in this review.

Real et al[98] Pistone et al[97] Coban et al[93] Lodagekar et al[82] Costabile et al[53] Bai et al[51] Yang et al[84] Such an approach enables to enhance the NIC solubility and its incorporation into more advanced formulations like 3D printlets, enabling dose individualization, or nanofibers that may be implanted into the body following the cancer surgery, to locally release the drug in a controllable manner thus preventing metastasis. Unfortunately, all these approaches are still at the proof of the concept level, requiring further investigation that might be pellicular for academia, considering the costs of pharmacokinetic, pharmacodynamic, and toxicological studies. Probably, the pharmaceutical industry should get more involved. In this light, it is surprising that there were no attempts to develop more self (micro)emulsifying formulations (SMEEDS) of NIC. The use of oils as solvents in combination with surfactants and co-solvents may aid in the solubility of NIC and enhance its oral bioavailability, as demonstrated by Zhang et al[68] Such a formulation is suitable for oral administration (as soft gelatine capsules) or injections and has the highest potential to enable the translation of NIC from academic research to clinical application. Another focus should be set on the antiviral activity of NIC, requiring the local administration of the drug dose in the lung by inhalation. At the moment, there are only a few works addressing this problem. Furthermore, investigating pulmonary delivery for systemic therapy is warranted to circumvent the degradation of NIC by hepatic enzymes. Another pertinent consideration is rectal delivery, primarily to mitigate the glucuronidation of NIC, but also to increase its solubility as the solubility of NIC increases with increasing pH values.[101] Incorporating these delivery methods into the study of NIC therapy could provide valuable insights into optimizing its systemic effects while minimizing metabolism and enhancing its bioavailability. However, it's crucial to conduct thorough research and clinical trials to evaluate the safety, efficacy, and feasibility of these delivery approaches for NIC and ensure their practicality in clinical settings.

Furthermore, many current studies, listed by Barbosa in his review paper[10] were performed by the administration of NIC as a hard gelatine capsule or as a commercially available chewable tablet (Yomesan ®), clearly underlays the lack of efficiency of such conventional formulations, urging the need for new and more efficient formulations. For the moment, liposomal NIC embedded into Poloxamer-based thermoreversible gel appears as the most probable formulation for further transfer to the clinic practice.[78] Incorporation of the drug into liposomes in combination with the thermogelling properties of the formulation ensures the prolonged topical delivery of the drug to the skin to treat melanoma, without exposing the drug to the systemic circulation, thereby avoiding systemic side effects. However, the real therapeutic potential of such a formulation must be verified through extensive clinical trials.

Conclusion

There is significant interest in repurposing NIC, as evidenced by the numerous efforts to enhance its solubility and consequently improve its bioavailability. Many studies have reported notable advancements in solubility and some have even demonstrated improved pharmacokinetics following in vivo administration. A significant portion of these studies has not undertaken in vivo pharmacokinetic assessments but are based on in vitro results. Therefore, the enhancements

observed in vivo remain unproven and require further validation. The fate of NIC is not solely determined by its solubility but also by its substantial first-pass metabolism in the intestine and liver, as indicated by studies, so the in vitro results are difficult to repeat in vivo. Given the considerable variability among these studies, identifying the most promising formulation remains challenging. Nonetheless, there is still room for additional exploration and new trials, including exploring alternative routes of administration such as topical, pulmonary, or rectal delivery, as well as investigating different formulation types like soft gelatin capsules.

Acknowledgments

The authors express their gratitude to Prof. Mauro Sambi from the Department of Chemical Sciences, University of Padova, for the assistance provided in obtaining the literature.

Disclosure

The authors report no conflicts of interest in this work.

References

1. Jara MO, Warnken ZN, Williams RO III. Amorphous solid dispersions and the contribution of nanoparticles to in vitro dissolution and in vivo testing: niclosamide as a case study. *Pharmaceutics*. 2021;13:97. doi:10.3390/pharmaceutics13010097
2. Jara MO, Williams RO III. The challenge of repurposing niclosamide: considering pharmacokinetic parameters, routes of administration, and drug metabolism. *J Drug Deliv Sci Technol*. 2023;81:104187. doi:10.1016/j.jddst.2023.104187
3. Naqvi S, Mohiyuddin S, Gopinath P. Niclosamide loaded biodegradable chitosan nanocargoes: an in vitro study for potential application in cancer therapy. *R Soc Open Sci*. 2017;4:170611. doi:10.1098/rsos.170611
4. Wu CJ, Jan JT, Chen CM, et al. Inhibition of severe acute respiratory syndrome coronavirus replication by niclosamide. *Antimicrob Agents Chemother*. 2004;48(7):2693–2696. doi:10.1128/aac.48.7.2693-2696.20
5. Jara MO, Warnken ZN, Sahakijpijarn S, et al. Niclosamide inhalation powder made by thin-film freezing: multi-dose tolerability and exposure in rats and pharmacokinetics in hamsters. *Int J Pharm*. 2021;603:120701. doi:10.1016/j.ijpharm.2021.120701
6. Russo A, Pellosi DS, Pagliara V, et al. Biotin-targeted Pluronic® P123/F127 mixed micelles delivering niclosamide: a repositioning strategy to treat drug-resistant lung cancer cells. *Int J Pharm*. 2016;511(1):127–139. doi:10.1016/j.ijpharm.2016.06.118
7. Yu S, Piao H, Rejinold NS, Jin G, Choi G, Choy JH. Niclosamide–clay intercalate coated with nonionic polymer for enhanced bioavailability toward COVID-19 treatment. *Polymers*. 2021;13:1044. doi:10.3390/polym13071044
8. Kapale SS, Chaudhari HK. Niclosamide & challenges in chemical modifications: a broad review on enhancement of solubility. *J Indian Chem Soc*. 2021;98(12):100262. doi:10.1016/j.jics.2021.100262
9. Jara MO, Warnken ZN, Sahakijpijarn S, et al. Oral delivery of niclosamide as an amorphous solid dispersion that generates amorphous nanoparticles during disso-lution. *Pharmaceutics*. 2022;1:2568. doi:10.3390/pharmaceutics14122568
10. Barbosa EJ, Löbenberg R, de Araujo GLB, Bou-Chacra NA. Niclosamide repositioning for treating cancer: challenges and nano-based drug delivery opportunities. *Eur J Pharm Biopharm*. 2019;141:58–69. doi:10.1016/j.ejpb.2019.05.004
11. Pardhi V, Chavan RB, Thipparaboina R, Thatikonda S, Naidu VGM, Shastri NR. Preparation, characterization, and cytotoxicity studies of niclosamide loaded mesoporous drug delivery systems. *Int J Pharm*. 2017;528(1–2):202–214. doi:10.1016/j.ijpharm.2017.06.007
12. Natera J, Gatica E, Challier C, et al. On the photooxidation of the multifunctional drug niclosamide. A kinetic study in the presence of vitamin B2 and visible light. *Redox Rep*. 2015;20(6):259–266. doi:10.1179/1351000215Y.0000000010
13. Johnsirani P, Ch V, Lingesh A, Naidu VGM, Ch N, Satheeshkumar N. Isolation, characterization using LC-ESI-QTOF, NMR and in vitro cytotoxicity assay of niclosamide forced degradation products. *J Pharm Biomed Anal*. 2017;136:148–155. doi:10.1016/j.jpba.2017.01.001
14. Osada T, Chen M, Yang XY, et al. Antihelminth compound niclosamide downregulates Wnt signaling and elicits antitumor responses in tumors with activating APC mutations. *Cancer Res*. 2011;71(12):4172–4182. doi:10.1158/0008-5472.CAN-10-3978
15. van Tonder EC, Maleka TS, Liebenberg W, Song M, Wurster DE, de Villiers MM. Preparation and physicochemical properties of niclosamide anhydrate and two monohydrates. *Int J Pharm*. 2004;269(2):417–432. doi:10.1016/j.ijpharm.2003.09.035
16. Harriss BI, Wilson C, Radosavljevic Evans I. Niclosamide methanol solvate and niclosamide hydrate: structure, solvent inclusion mode and implications for properties. *Acta Crystallogr Sect C*. 2014;70(8):758–763. doi:10.1016/j.ijpharm.2003.09.035
17. Arnott JA, Planey SL. The influence of lipophilicity in drug discovery and design. *Expert Opini Drug Discov*. 2012;7(10):863–875. doi:10.1517/17460441.2012.714363
18. Mu H, Holm R, Müllertz A. Lipid-based formulations for oral administration of poorly water-soluble drugs. *Int J Pharm*. 2013;453(1):215–224. doi:10.1016/j.ijpharm.2013.03.054
19. Williams HD, Trevaskis NL, Yeap YY, Anby MU, Pouton CW, Porter CJ. Lipid-based formulations and drug supersaturation: harnessing the unique benefits of the lipid digestion/absorption pathway. *Pharma Res*. 2013;30:2976–2992. doi:10.1007/s11095-013-1126-0
20. Seo JI, Jin GW, Yoo HH. Pharmacokinetic considerations for enhancing drug repurposing opportunities of anthelmintics: niclosamide as a case study. *Biomed Pharmacother*. 2024;173:116394. doi:10.1016/j.biopha.2024.116394
21. Lu D, Ma Z, Zhang T, Zhang X, Wu B. Metabolism of the anthelmintic drug niclosamide by cytochrome P450 enzymes and UDP-glucuronosyltransferases: metabolite elucidation and main contributions from CYP1A2 and UGT1A1. *Xenobiotica*. 2016;46(1):1–13. doi:10.3109/00498254.2015.1047812
22. Fan X, Li H, Ding X, Zhang QY. Contributions of hepatic and intestinal metabolism to the disposition of niclosamide, a repurposed drug with poor bioavailability. *Drug Met Dis*. 2019;47(7):756–763. doi:10.1124/dmd.119.086678

23. Choi HI, Kim T, Lee SW, et al. Bioanalysis of niclosamide in plasma using liquid chromatography-tandem mass and application to pharmacokinetics in rats and dogs. *J Chrom B*. 2021;1179:122862. doi:10.1016/j.jchromb.2021.122862
24. Ohno S, Nakajin S. Determination of mRNA expression of human UDP-glucuronosyltransferases and application for localization in various human tissues by real-time reverse transcriptase-polymerase chain reaction. *Drug Met Dis*. 2009;37(1):32–40. doi:10.1124/dmd.108.023598
25. Ye Y, Zhang X, Zhang T, Wang H, Wu B. Design and evaluation of injectable niclosamide nanocrystals prepared by wet media milling technique. *Drug Dev Ind Pharm*. 2015;41(9):1416–1424. doi:10.3109/03639045.2014.954585
26. Tao H, Zhang Y, Zeng X, Shulman GI, Jin S. Niclosamide ethanolamine–induced mild mitochondrial uncoupling improves diabetic symptoms in mice. *Nat Med*. 2014;20(11):1263–1269. doi:10.1038/nm.3699
27. Schweizer MT, Haugk K, McKiernan JS, et al. A phase I study of niclosamide in combination with enzalutamide in men with castration-resistant prostate cancer. *PLoS One*. 2018;13(6):e0198389. doi:10.1371/journal.pone.0198389
28. Parikh M, Liu C, Wu CY, et al. Phase Ib trial of reformulated niclosamide with Abiraterone/prednisone in men with castration-resistant prostate cancer. *Sci Rep*. 2011;11(1):6377. doi:10.1038/s41598-021-85969-x
29. Singh S, Weiss A, Goodman J, et al. Niclosamide—A promising treatment for COVID-19. *Br J Pharmacol*. 2022;179(13):3250–3267. doi:10.1111/bph.15843
30. Yang M, Wang AQ, Padilha EC, et al. Use of physiological based pharmacokinetic modeling for cross-species prediction of pharmacokinetic and tissue distribution profiles of a novel niclosamide prodrug. *Front Pharmacol*. 2023;14:1099425. doi:10.3389/fphar.2023.1099425
31. Chen H, Yang Z, Ding C, et al. Discovery of O-alkylamino-tethered niclosamide derivatives as potent and orally bioavailable anticancer agents. *ACS Med Chem Lett*. 2013;4(2):180–185. doi:10.1021/ml3003082
32. Xu J, Pachón-Ibáñez ME, Cebrero-Cangueiro T, Chen H, Sánchez-Céspedes J, Zhou J. Discovery of niclosamide and its O-alkylamino-tethered derivatives as potent antibacterial agents against carbapenemase-producing and/or colistin resistant Enterobacteriaceae isolates. *Bioorg Med Chem Lett*. 2019;29(11):1399–1402. doi:10.1016/j.bmcl.2019.03.032
33. Ma R, Ma ZG, Gao JL, et al. Injectable pegylated niclosamide (polyethylene glycol-modified niclosamide) for cancer therapy. *J Biomed Mater Res A*. 2020;108(1):30–38. doi:10.1002/jbm.a.36788
34. He X, Li M, Ye W, Zhou W. Discovery of degradable niclosamide derivatives able to specially inhibit small cell lung cancer (SCLC). *Bioorg Chem*. 2021;107:104574. doi:10.1016/j.bioorg.2020.104574
35. Wu CL, Chen CL, Huang HS, Yu DS. A new niclosamide derivatives-B17 can inhibit urological cancers growth through apoptosis-related pathway. *Cancer Med*. 2018;7(8):3945–3954. doi:10.1002/cam4.1635
36. Li Z, Xu J, Lang Y, et al. JMX0207, a niclosamide derivative with improved pharmacokinetics, suppresses zika virus infection both in vitro and in vivo. *ACS Infect Dis*. 2020;6(10):2616–2628. Epub 2020 Sep 21. PMID: 32866370. doi:10.1021/acsinfecdis.0c00217
37. Mook RA Jr, Wang J, Ren XR, et al. Structure–activity studies of Wnt/β-catenin inhibition in the Niclosamide chemotype: identification of derivatives with improved drug exposure. *Bioorg Med Chem*. 2015;23(17):5829–5838. doi:10.1016/j.bmc.2015.07.001
38. Shamim K, Xu M, Hu X, et al. Application of niclosamide and analogs as small molecule inhibitors of Zika virus and SARS-CoV-2 infection. *Bioorg Med Chem Lett*. 2021;40:127906. doi:10.1016/j.bmcl.2021.127906
39. Alasadi A, Chen M, Swapna GVT, et al. Effect of mitochondrial uncouplers niclosamide ethanolamine (Nen) and oxyclozanide on hepatic metastasis of colon cancer. *Cell Death Dis*. 2018;9(2):215. doi:10.1038/s41419-017-0092-6
40. Bhanushali JS, Dhiman S, Nandi U, Bharate SS. Molecular interactions of niclosamide with hydroxyethyl cellulose in binary and ternary amorphous solid dispersions for synergistic enhancement of water solubility and oral pharmacokinetics in rats. *Int J Pharm*. 2022;626:122144. doi:10.1016/j.ijpharm.2022.122144
41. Schittny A, Huwyler J, Puchkov M. Mechanisms of increased bioavailability through amorphous solid dispersions: a review. *Drug Deliv*. 2020;27(1):110–127. doi:10.1080/10717544.2019.1704940
42. Indulkar AS, Lou X, Zhang GG, Taylor LS. Insights into the dissolution mechanism of ritonavir–copovidone amorphous solid dispersions: importance of congruent release for enhanced performance. *Mol Pharm*. 2019;16(3):1327–1339. doi:10.1021/acs.molpharmaceut.8b01261
43. Thakkar R, Thakkar R, Pillai A, Ashour EA, Repka MA. Systematic screening of pharmaceutical polymers for hot melt extrusion processing: a comprehensive review. *Int J Pharm*. 2020;576:118989. doi:10.1016/j.ijpharm.2019.118989
44. Ray E, Vaghasiya K, Sharma A, et al. Autophagy-inducing inhalable co-crystal formulation of niclosamide-nicotinamide for lung cancer therapy. *AAPS Pharm Sci Tech*. 2020;21:1–14. doi:10.1208/s12249-020-01803-z
45. Shan N, Perry ML, Weyna DR, Zaworotko MJ. Impact of pharmaceutical co-crystals: the effects on drug pharmacokinetics. *Expert Opin Drug Metab Toxicol*. 2014;10(9):1255–1271. doi:10.1517/17425255.2014.942281
46. Luedeker D, Gossmann R, Langer K, Brunklaus G. Crystal engineering of pharmaceutical co-crystals:"NMR crystallography" of niclosamide co-crystals. *Cryst Growth Des*. 2016;16(6):3087–3100. doi:10.1021/acs.cgd.5b01619
47. Grifasi F, Chierotti MR, Gaglioti K, et al. Using salt co-crystals to improve the solubility of niclosamide. *Cryst Growth Des*. 2015;15 (4):1939–1948. doi:10.1021/acs.cgd.5b00106
48. Sanphui P, Kumar SS, Nangia A. Pharmaceutical co-crystals of niclosamide. *Cryst Growth Des*. 2012;12(9):4588–4599. doi:10.1021/cg300784v
49. D'Abbrunzo I, Bianco E, Gigli L, et al. Praziquantel meets niclosamide: a dual-drug antiparasitic co-crystal. *Int J Pharm*. 2023;644:123315. doi:10.1016/j.ijpharm.2023.123315
50. Lin CK, Bai MY, Hu TM, et al. Preclinical evaluation of a nanoformulated antihelminthic, niclosamide, in ovarian cancer. *Oncotarget*. 2016;7 (8):8993. doi:10.18632/oncotarget.7113
51. Bai MY, Yang HC. Fabrication of novel niclosamide-suspension using an electrospray system to improve its therapeutic effects in ovarian cancer cells in vitro. *Colloid Surf A*. 2013;419:248–256. doi:10.1016/j.colsurfa.2012.11.076
52. Sardo M, Amado AM, Ribeiro-Claro PJ. Pseudopolymorphic transitions of niclosamide monitored by Raman spectroscopy. *J Raman Spectrosc*. 2008;39(12):1915–1924. doi:10.1002/jrs.2058
53. Costabile G, d'Angelo I, Rampioni G, et al. Toward repositioning niclosamide for antivirulence therapy *of Pseudomonas aeruginosa* lung infections: development of inhalable formulations through nanosuspension technology. *Mol Pharm*. 2015;12(8):2604–2617. doi:10.1021/acs.molpharmaceut.5b00098

54. Brunaugh AD, Seo H, Warnken Z, Ding L, Seo SH, Smyth HD. Development and evaluation of inhalable compo-site niclosamide-lysozyme particles: a broad-spectrum, patient-adaptable treatment for coronavirus infections and sequalae. *PLoS One*. 2021;16(2):e0246803. doi:10.1371/journal.pone.0246803
55. Hobson JJ, Savage AC, Dwyer AB, et al. Scalable nanoprecipitation of niclosamide and in vivo demonstration of long-acting delivery after intramuscular injection. *Nanoscale*. 2021;13(13):6410–6416. doi:10.1039/D1NR00309G
56. Biswas S, Kumari P, Lakhani PM, Ghosh B. Recent advances in polymeric micelles for anti-cancer drug delivery. *Eur J Pharm Sci*. 2016;83:184–202. doi:10.1016/j.ejps.2015.12.031
57. Hang J, Chen Y, Tian P, Yu R, Wang M, Zhao M. Preparation and pharmacodynamics of niclosamide micelles. *J Drug Deliv Sci Technol*. 2022;68:103088. doi:10.1016/j.jddst.2021.103088
58. Bhattacharyya J, Ren XR, Mook RA, et al. Niclosamide-conjugated polypeptide nanoparticles inhibit Wnt signaling and colon cancer growth. *Nanoscale*. 2017;9(34):12709–12717. doi:10.1039/C7NR01973D
59. Misra SK, Jensen TW, Pan D. Enriched inhibition of cancer and stem-like cancer cells via STAT-3 modulating niclocelles. *Nanoscale*. 2015;7(16):7127–7132. doi:10.1039/C5NR00403A
60. Wang J, Song Y. Microfluidic synthesis of nanohybrids. *Small*. 2017;13(18):1604084. doi:10.1002/smll.201604084
61. Zhao N, Yan L, Zhao X, et al. Versatile types of organic/inorganic nanohybrids: from strategic design to biomedical applications. *Chem Rev*. 2018;119(3):1666–1762. doi:10.1021/acs.chemrev.8b00401
62. Choi G, Piao H, Rejinold NS, et al. Hydrotalcite–niclosamide nanohybrid as oral formulation towards SARS-CoV-2 viral infections. *Pharmaceuticals*. 2021;14:486. doi:10.3390/ph14050486
63. Piao H, Rejinold NS, Choi G, Pei YR, Jin GW, Choy JH. Niclosamide encapsulated in mesoporous silica and geo-polymer: a potential oral formulation for COVID-19. *Microporous Mesoporous Mat*. 2021;326:111394. doi:10.1016/j.micromeso.2021.111394
64. Rejinold NS, Choi G, Piao H, Choy JH. Bovine serum albumin-coated niclosamide-zein nanoparticles as potential injectable medicine against COVID-19. *Materials*. 2021;14:3792. doi:10.3390/ma14143792
65. Nayar S, Mir A, Ashok A, Guha A, Sharma V. Bovine serum albumin binding and drug delivery studies with PVA-ferrofluid. *J Bionic Eng*. 2010;7(1):29–34. doi:10.1016/S1672-6529(09)60188-8
66. Rejinold NS, Piao H, Jin GW, Choi G, Choy JH. Injectable niclosamide nanohybrid as an anti-SARS-CoV-2 strategy. *Colloids and Surf B*. 2021;208:112063. doi:10.1016/j.colsurfb.2021.112063
67. Rejinold NS, Piao H, Choi G, Jin GW, Choy JH. Niclosamide-exfoliated anionic clay nanohybrid repurposed as an antiviral drug for tackling Covid-19; oral formulation with tween 60/eudragit s100. *Clays Clay Miner*. 2021;1–14. doi:10.1007/s42860-021-00153-6
68. Lingayat VJ, Zarekar NS, Shendge RS. Solid lipid nanoparticles: a review. *Nanosci Nanotechnol Res*. 2017;4(2):67–72. doi:10.12691/nnr-4-2-5
69. Liu P, Chen G, Zhang J. A review of liposomes as a drug delivery system: current status of approved products, regulatory environments, and future perspectives. *Molecules*. 2022;27:1372. doi:10.3390/molecules27041372
70. Zhang X, Zhang Y, Zhang T, Zhang J, Wu B. Significantly enhanced bioavailability of niclosamide through submicron lipid emulsions with or without PEG-lipid: a comparative study. *J Microencapsul*. 2015;32(5):496–502. doi:10.3109/02652048.2015.1057251
71. Yáñez JA, Wang SW, Knemeyer IW, Wirth MA, Alton KB. Intestinal lymphatic transport for drug delivery. *Adv Drug Deliv Rev*. 2011;63(10–11):923–942. doi:10.1016/j.addr.2011.05.019
72. Naseri N, Valizadeh H, Zakeri-Milani P. Solid lipid nanoparticles and nanostructured lipid carriers: structure, preparation and application. *Adv Pharm Bull*. 2015;5(3):305. doi:10.15171/apb.2015.043
73. Rehman MU, Khan MA, Khan WS, Shafique M, Khan M. Fabrication of Niclosamide loaded solid lipid nanoparticles: *in vitro* characterization and comparative *in vivo* evaluation. *Artif Cells Nanomed Biotechnol*. 2018;46(8):1926–1934. doi:10.1080/21691401.2017.1396996
74. Pindiprolu SKS, Chintamaneni PK, Krishnamurthy PT, Ratna Sree Ganapathineedi K. Formulation-optimization of solid lipid nanocarrier system of STAT3 inhibitor to improve its activity in triple negative breast cancer cells. *Drug Dev Ind Pharm*. 2019;45(2):304–313. doi:10.1080/03639045.2018.1539496
75. Wang G, Gaikwad H, McCarthy MK, et al. Lipid nanoparticle formulation of niclosamide (nano NCM) effectively inhibits SARS-CoV-2 replication in vitro. *Precis Nanomed*. 2021;4(1):724. doi:10.33218/001c.18813
76. Yu Y, Liu H, Yuan L, et al. Niclosamide-encapsulated lipid nanoparticles for the reversal of pulmonary fibrosis. *Mater Today Bio*. 2024;25:100980. doi:10.1016/j.mtbio.2024.100980
77. Reddy GB, Kerr DL, Spasojevic I, et al. Preclinical testing of a novel niclosamide stearate prodrug therapeutic (NSPT) shows efficacy against osteosarcoma. *Mol Cancer Ther*. 2020;19(7):1448–1461. doi:10.1158/1535-7163.MCT-19-0689
78. Shah S, Famta P, Fernandes V, et al. Quality by de-sign steered development of niclosamide loaded liposomal thermogel for melanoma: in vitro and ex vivo evaluation. *Eur J Pharm Biopharm*. 2022;180:119–136. doi:10.1016/j.ejpb.2022.09.024
79. Elkholy NE, Sultan AA, Abu-Risha SE, El Maghraby GM. Chitosan coated lipid carriers as nanoplatform for repurposed anti-breast cancer activity of niclosamide. *J Drug Deliv Sci Technol*. 2024;93:105414. doi:10.1016/j.jddst.2024.105414
80. Stella VJ, He Q. Cyclodextrins. *Toxicol Pathol*. 2008;36(1):30–42. doi:10.1177/019262330731094
81. Patel AR, Vavia PR. Preparation and evaluation of taste masked famotidine formulation using drug/β-cyclodextrin/polymer ternary complexation approach. *AAPS Pharm Sci Tech*. 2008;9:544–550. doi:10.1208/s12249-008-9078-0
82. Lodagekar A, Borkar RM, Thatikonda S, et al. Formulation and evaluation of cyclodextrin complexes for improved anticancer activity of repurposed drug: niclosamide. *Carbohydr Polym*. 2019;212:252–259. doi:10.1016/j.carbpol.2019.02.041
83. Xie Y, Yao Y. Octenylsuccinate hydroxypropyl phytoglycogen enhances the solubility and in-vitro antitumor efficacy of niclosamide. *Int J Pharm*. 2018;535(1–2):157–163. doi:10.1016/j.ijpharm.2017.11.004
84. Yang W, de Villiers MM. Effect of 4-sulphonato-calix [n] arenes and cyclodextrins on the solubilization of niclosamide, a poorly water soluble anthelmintic. *AAPS*. 2005;7:E241–E248. doi:10.1208/aapsj070123
85. Bhardwaj H, Jangde RK. Current updated review on preparation of polymeric nanoparticles for drug delivery and biomedical applications. *Next Nanotechnol*. 2023;2:100013. doi:10.1016/j.nxnano.2023.100013
86. Gan C, Wang Y, Xiang Z, et al. Niclosamide-loaded nanoparticles (Ncl-NPs) reverse pulmonary fibrosis in vivo and in vitro. *J Adv Res*. 2023;51:109–120. doi:10.1016/j.jare.2022.10.018

87. Bhushan B, Dubey P, Kumar SU, Sachdev A, Matai I, Gopinath P. Bionanotherapeutics: niclosamide encapsulated albumin nanoparticles as a novel drug delivery system for cancer therapy. *RSC Adv*. 2015;5(16):12078–12086. doi:10.1039/C4RA15233F
88. Misra SK, Wang X, Srivastava I, et al. Combinatorial therapy for triple negative breast cancer using hyperstar polymer-based nanoparticles. *Chem Comm*. 2015;51(93):16710–16713. doi:10.1039/C5CC07709E
89. Luraghi A, Peri F, Moroni L. Electrospinning for drug delivery applications: a review. *J Control Release*. 2021;334:463–484. doi:10.1016/j.jconrel.2021.03.033
90. Kumar SU, Gopinath P. Controlled delivery of bPEI–niclosamide complexes by PEO nanofibers and evaluation of its anti-neoplastic potentials. *Colloids Surf B*. 2015;131:170–181. doi:10.1016/j.colsurfb.2015.04.063
91. Dubey P, Gopinath P. Fabrication of electrospun poly (ethylene oxide)–poly (capro lactone) composite nanofibers for co-delivery of niclosamide and silver nanoparticles exhibits enhanced anti-cancer effects in vitro. *J Mater Chem B*. 2016;4(4):726–742. doi:10.1039/C5TB02351C
92. Sukumar UK, Gopinath P. Field-actuated antineoplastic potential of smart and versatile PEO–bPEI electrospun scaffold by multi-staged targeted co-delivery of magnetite nanoparticles and niclosamide–bPEI complexes. *RSC Adv*. 2016;6(52):46186–46201. doi:10.1039/C6RA05006A
93. Coban O, Aytac Z, Yildiz ZI, Uyar T. Colon targeted delivery of niclosamide from β-cyclodextrin inclusion complex incorporated electrospun Eudragit® L100 nanofibers. *Colloids Surf B*. 2021;197:111391. doi:10.1016/j.colsurfb.2020.111391
94. Chaurasiya B, Zhao YY. Dry powder for pulmonary delivery: a comprehensive review. *Pharmaceutics*. 2021;13:31. doi:10.3390/pharmaceutics13010031
95. Weers JG, Miller DP. Formulation design of dry powders for inhalation. *J Pharm Sci*. 2015;104(10):3259–3288. doi:10.1002/jps.24574
96. Okafor-Muo OL, Hassanin H, Kayyali R, ElShaer A. 3D printing of solid oral dosage forms: numerous challenges with unique opportunities. *J Pharm Sci*. 2020;109(12):3535–3550. doi:10.1016/j.xphs.2020.08.029
97. Pistone M, Racaniello GF, Arduino I, et al. Direct cyclodextrin-based powder extrusion 3D printing for one-step production of the BCS class II model drug niclosamide. *Drug Delivery Trans Res*. 2022;12(8):1895–1910. doi:10.1007/s13346-022-01124-7
98. Real JP, Real DA, Lopez-Vidal L, et al. 3D-printed gastroretentive tablets loaded with niclosamide nanocrystals by the melting solidification printing process (MESO-PP). *Pharmaceutics*. 2023;15:1387. doi:10.3390/pharmaceutics15051387
99. Wang Z, Ren J, Du J, Wang H, Liu J, Wang G. Niclosamide as a promising therapeutic player in human cancer and other diseases. *Int J Mol Sci*. 2022;23:16116. doi:10.3390/ijms232416116
100. Ren J, Wang B, Wu Q, Wang G. Combination of niclosamide and current therapies to overcome resistance for cancer: new frontiers for an old drug. *Biomed Pharmacother*. 2022;155:113789. doi:10.1016/j.biopha.2022.113789
101. Needham D. The PH dependence of niclosamide solubility, dissolution, and morphology: motivation for potentially universal mucin-penetrating nasal and throat sprays for COVID19, its variants and other viral infections. *Pharma Res*. 2022;39(1):115–141. doi:10.1007/s11095-021-03112-x